RECEIVED
LIBRARY
LAWRENCE RADIATION LABORATORY

UCRL-20480 c.2

DOCUMENTS SECTION

ISOSPIN PURITY AND VIOLATIONS OF MIRROR SYMMETRY: THE BETA-DELAYED PROTON DECAY OF ^{9}C, ^{13}O, ^{17}Ne, AND ^{33}Ar

John Edward Esterl
(Ph. D. Thesis)

March 1971

AEC Contract No. W-7405-eng-48

TWO-WEEK LOAN COPY

This is a Library Circulating Copy which may be borrowed for two weeks. For a personal retention copy, call Tech. Info. Division, Ext. 5545

LAWRENCE RADIATION LABORATORY
UNIVERSITY of CALIFORNIA BERKELEY

UCRL-20480 c.2

DISCLAIMER

This document was prepared as an account of work sponsored by the United States Government. While this document is believed to contain correct information, neither the United States Government nor any agency thereof, nor the Regents of the University of California, nor any of their employees, makes any warranty, express or implied, or assumes any legal responsibility for the accuracy, completeness, or usefulness of any information, apparatus, product, or process disclosed, or represents that its use would not infringe privately owned rights. Reference herein to any specific commercial product, process, or service by its trade name, trademark, manufacturer, or otherwise, does not necessarily constitute or imply its endorsement, recommendation, or favoring by the United States Government or any agency thereof, or the Regents of the University of California. The views and opinions of authors expressed herein do not necessarily state or reflect those of the United States Government or any agency thereof or the Regents of the University of California.

ISOSPIN PURITY AND VIOLATIONS OF MIRROR SYMMETRY: THE BETA-DELAYED PROTON DECAY OF ^{9}C, ^{13}O, ^{17}Ne, AND ^{33}Ar

Contents

Abstract v

I. Introduction 1

II. Theory: Beta-Decay and Isospin Purity 6

A. Superallowed and Allowed Beta-Decay 6

B. First-Forbidden Beta-Decay 10

C. Induced Tensor Coupling in Beta-Decay? 11

III. Experimental Methods 24

A. Cyclotron and Beam Transport 24

B. The Pulsed-Beam, Shielded-Detector Method 24

C. Gas-Sweeping System 31

D. Electronics and Counting Techniques 36

E. Half-life Measurements 42

IV. Experimental Results 44

A. ^{33}Ar Decay 44

B. ^{17}Ne Decay 56

C. ^{13}O Decay 77

D. ^{9}C Decay 84

V. Conclusions 91

A. Isospin Purity 91

B. Antianalogue States 94

VI. Summary 97

Acknowledgments 99

Appendices. 100

A. Cross Section Formula. 100

B. Beta-Broadening of the Delayed-Proton Peaks. 103

References and Footnotes. 105

ISOSPIN PURITY AND VIOLATIONS OF MIRROR SYMMETRY: THE BETA-DELAYED PROTON DECAY OF ^{9}C, ^{13}O, ^{17}Ne, AND ^{33}Ar

John Edward Esterl

Department of Chemistry and
Lawrence Radiation Laboratory
University of California
Berkeley, California 94720

March 1971

ABSTRACT

Beta-delayed proton studies of some light $A = 4n+1$, $T_z = -3/2$ nuclei have been made. Supplementary γ-ray measurements were made where necessary. A fast gas-transport system and particle-identification techniques combined to produce proton spectra in which the resolution was limited by the momentum spread of the preceding beta-ray. The half-lives measured are: ^{9}C, 126.5 ± 1.0 ms; ^{13}O, 8.95 ± 0.20 ms; ^{17}Ne, 109.0 ± 1.0 ms; and ^{33}Ar, 173.0 ± 2.0 ms. Precise level energies in ^{17}F and ^{33}Cl have been measured and a discrepancy concerning levels in ^{17}F has been resolved. Absolute log ft-values for the β-decay branches of ^{13}O, ^{17}Ne, and ^{33}Ar have been obtained; these measurements indicate violations of mirror symmetry in beta-decay. They also indicate that the lowest $T = 3/2$ state in ^{17}F has an isospin purity of $\geqslant 95\%$, in contrast to the lowest $T = 3/2$ state in ^{33}Cl, for which an impurity of $\sim 10\%$ is suggested. Circumstantial evidence indicates that four $T = 1/2$ states within 350 keV of the analogue state cause the impurity observed in ^{33}Cl.

I. INTRODUCTION

Many of the levels fed by the β^+-decay of the $T = 3/2$, $T_z = -3/2$ nuclei ^9C, ^{13}O, ^{17}Ne, and ^{33}Ar, lie above the proton separation energy of the daughter nucleus. Upon formation these levels decay virtually instantaneously by emitting "delayed protons". The unifying theme of this research is the detection of these protons, although the types of information obtained vary from case to case. Measurement of the energies of these proton groups determines the location of energy levels in the daughter nucleus. In some cases analysis of the intensities of the groups yields absolute ft-values, from which certain conclusions concerning isospin purity, mirror symmetry in β-decay, and other interesting topics can be deduced.

If all the β^+-transitions lead to proton-unstable states, absolute ft-values can be determined from the relative intensities of the proton groups. This is approximately true in the decay of ^{17}Ne because the two beta transitions to states below the proton-separation energy in ^{17}F are first-forbidden. In other cases a combination of γ-ray measurements and calculations based on mirror β^--transitions is required to obtain absolute ft-values. The high sensitivity and efficiency of charged-particle detectors makes it possible to characterize very weak β^+-decay branches with high precision. Background from other nuclei is rarely a problem, because the combination of high β-decay energy and relatively low proton-separation energy that allows delayed-proton emission does not occur often.

A test of mirror symmetry in β-decay is provided by comparing ft-values for the decays of these neutron deficient nuclei with data from the decay of their mirrors. Since mirror nuclei have virtually identical wave

functions, the ft-values for their decays should be equal. However, the ft-values for decay of the mirror nuclei ^{12}N and ^{12}B differ by about 10% and calculations of electromagnetic and other effects have failed to explain this deviation from mirror symmetry.[1]

The existence of an induced tensor term in beta-decay has been suggested[2,3] as a possible explanation for this phenomenon. Such a term is expected[4] to increase in effect as the decay energy increases. The light delayed-proton emitters have high decay energies, making a study of their beta-decays particularly interesting.

The superallowed beta-decay from the T = 3/2 parent nucleus to its known[5] T = 3/2 analogue state in the daughter was observed for both ^{17}Ne and ^{33}Ar. Such superallowed transitions have low log ft-values and are calculable--to a few percent--model independently. This calculation assumes the wave functions of the initial and final states to be identical. Since the analogue state in the $T_z = -1/2$ daughter nucleus is surrounded by many T = 1/2 states and the Coulomb force does not conserve isobaric spin, some mixing must occur. Comparison of the observed ft-value for the superallowed transition to the calculated value should yield a measure of that mixing.

Table I lists[6-34] the known light delayed-particle emitters and shows one of the problems associated with their study, short half-lives. This property forced previous studies[21,23-27,31,32] of the four nuclei described herein to use unshielded detectors, looking directly at the target, and pulsed beams. The resulting spectra exhibited poor resolution, substantial background, and a cutoff for low-energy ($E_{lab} \leqslant 2.5$ MeV)

Table I. Known delayed charged-particle emitters of mass $\leqslant 60$.[a]

Mass series	T_z	Nucleus	Half-life (ms)	Activity	Reference(s)
4n	+1	^{8}Li	850 ± 4	α	6,7
		^{12}B	20.41 ± 0.06	α	8,9
		^{16}N	7130 ± 20	α	10,11
	-1	^{8}B	774 ± 4	α	6,12
		^{12}N	10.97 ± 0.04	α	8,9
		^{20}Na	451 ± 2[b]	α	13,14,15
		^{24}Al	2081 ± 9	α	16,17
		$^{24}Al^{m}$	129 ± 5	α	16,18,19
		^{32}Cl	298 ± 1	p,α	16,17
		^{40}Sc	182.7 ± 0.8	p	16,20
4n+1	-3/2	^{9}C	126.5 ± 0.9	p	21,22,c
		^{13}C	8.9 ± 0.2	p	23,c
		^{17}Ne	109 ± 1.0[d]	p	24,25,26,27,c
		^{21}Mg	121 ± 5	p	26,28
		^{25}Si	218 ± 4	p	26,29
		^{29}S	189 ± 7	p	25,28,30
		^{33}Ar	173.0 ± 2.0[d]	p	31,32,c
		^{37}Ca	174.6 ± 3.1	p	31,33
		^{41}Ti	88 ± 1	p	31
		^{49}Fe	75 ± 10	p	34

[a]The nucleus $^{53}Co^{m}$ is not tabulated since it has been found to exhibit true proton radioactivity with a half-life of 243 ± 15 ms. K. P. Jackson, C. U.

(continued)

Table I (continued)

Cardinal, H. C. Evans, N. A. Jelley, and J. Cerny, Phys. Letters 33B, 281 (1970), and J. Cerny, J. E. Esterl, R. A. Gough, and R. G. Sextro, Phys. Letters 33B, 284 (1970).

[b]Ref. 15 only.

[c]Present work.

[d]Present work only.

protons. Two devices were designed that attempted to solve these problems. The initial one, a rotating shield for the detectors, provided some improvement but for the nuclei reported here was inferior to the second, a fast gas-transport system. The latter transported the delayed-proton precursors of interest from the target position to a distant well-shielded counting chamber. Use of a cooled counter telescope and particle identification produced high resolution proton spectra. From these spectra and from accompanying γ- and p-γ coincidence measurements, absolute ft values were obtained for many branches, including superallowed decays from ^{17}Ne and ^{33}Ar.

II. THEORY: BETA-DECAY AND ISOSPIN PURITY

A. Superallowed and Allowed Beta-Decay

Beta-decay theory relates the observed strength of a particular β-transition to various properties of the states involved, such as spin, parity, and isospin purity. Theory also provides various selection rules and, for a superallowed decay, provides a very simple way of predicting the main part of its strength.

The strength of any β-transition is usually expressed in terms of its ft-value. The factor f takes account of the dependence of the transition strength on the energy release and on the nuclear charge. The partial half-life t is determined experimentally from the measured half-life and the fraction of all decays that proceed via the branch of interest. The ft value for allowed decay can then be related to the nuclear matrix elements:[35]

$$ft = \frac{2\pi^3(\ln 2)(\hbar^7/m^5c^4)}{g'^2_V\langle 1\rangle^2 + g'^2_A\langle\sigma\rangle^2} = \frac{6.15(10)^3}{\langle 1\rangle^2 + 1.50\langle\sigma\rangle^2}\ \text{sec.} \qquad (1)$$

In this expression g_V and g_A are the usual vector and axial vector coupling constants. The symbols $\langle 1\rangle$ and $\langle\sigma\rangle$ represent the Fermi and Gamow-Teller matrix elements, respectively. The coupling constants are primed to indicate that electromagnetic radiative corrections renormalize the coupling constants. This correction is small and unimportant for comparison of mirror decays where a ratio of ft-values is taken. However, in cases where one wishes to calculate the partial half-life of a particular transition, use of the renormalized constants has a significant effect, particularly on the ratio of the axial vector and vector coupling constants.

The Fermi matrix element for a β^+-transition between an initial state $|\psi_i(J_i, T_i)\rangle$ with spin and isospin (J_i, T_i) and a final state $|\psi_f(J_f, T_f)\rangle$ is given by:

$$\langle 1 \rangle = \langle \psi_f(J_f, T_f) | \sum_n \tau_+(n) | \psi_i(J_i, T_i) \rangle \quad , \tag{2}$$

where τ_+ is the isospin raising operator which changes a proton into a neutron and the summation extends over all n nucleons. From this matrix element the selection rules for superallowed decay are

$$J_f = J_i$$

$$T_f = T_i \quad . \tag{3}$$

In order to examine the effects of isospin mixing, consider the isospin-mixed final-state wave function $|\chi_f(J_f)\rangle$ written:

$$|\chi_f(J_f)\rangle = a|\psi_f^a(J_f, T)\rangle + b|\psi_f^b(J_f, T-1)\rangle \quad , \tag{4}$$

where the coefficients must be normalized. Using this wave function and Eq. (2), the Fermi matrix element squared is simply

$$\langle 1 \rangle^2 = [T(T+1) - T_{z_i} T_{z_f}]a^2 \quad , \tag{5}$$

where $\psi_f^a(J_f, T)$ is taken to be identical to $\psi_i(J_i, T)$. For the case of ^{17}Ne and ^{33}Ar, $T_i = 3/2$, and $T_{z_i} = -3/2$, so Eq. (5) yields

$$\langle 1 \rangle^2 = 3a^2 \quad . \tag{6}$$

When χ_f is the wave function of the analogue state, a^2 then represents the isospin purity of that state. This result requires the assumption that the basis wave function ψ_f^a is identical to ψ_i. This will be true provided all charge-dependent forces are small compared to the nuclear force, a reasonable assumption.

Analysis using the Fermi matrix element can be model independent since the transition operator does not alter the wave function. This is not the case for the Gamow-Teller matrix element which is given by

$$\langle \sigma \rangle = \langle \psi_f(J_f, T_f) | \sum_n \sigma(n)\tau_+(n) | \psi_i(J_i, T_i) \rangle \quad , \tag{7}$$

where $\sigma(n)$ is the Pauli spin vector. Evaluation of this matrix element requires explicit knowledge of the wave functions. Calculation of the wave functions in turn requires a particular model of the nucleus.

The selection rules for allowed decay are

$$\begin{array}{l} |J_f - J_i| = 0, 1 \\ \\ |T_f - T_i| = 0, 1 \end{array} \qquad 0 \not\longrightarrow 0 \quad . \tag{8}$$

These selection rules are satisfied by the superallowed decay branches in ^{17}Ne and ^{33}Ar. Therefore, an estimate of the contribution of the Gamow-Teller matrix element must be made. Calculations[36] of $\langle \sigma \rangle^2$ using the Nilsson model have been made and compared with experiment for eleven $T = 1/2$ mirror transitions in the range $17 \leqslant A \leqslant 39$. The agreement found was quite good. Similar calculations[36] for the decays of interest yield

$$\langle \sigma \rangle^2 = 0.11 \qquad {}^{17}\mathrm{Ne}$$
$$= 0.28 \qquad {}^{33}\mathrm{Ar} \quad . \tag{9}$$

Since the Fermi matrix element is quite large for T = 3/2 superallowed transitions, a 10% error in $\langle \sigma \rangle^2$ will contribute only 1% to the predicted ft-value. Thus, while the calculation of $\langle \sigma \rangle^2$ requires a model and may therefore be somewhat in error, the resulting ft prediction should be quite accurate. Finally, an upper limit can be set on the ft-value for the superallowed decay by assuming $\langle \sigma \rangle = 0$. This prediction is

$$\underline{ft} \leqslant 2.05 \times 10^3 \text{ sec} \quad (T_i = 3/2) \quad , \tag{10}$$

and any experimental violation of this limit must arise from isospin impurities.

Any isospin mixing in the analogue state will, of course, be accompanied by isospin impurities in T_{lower} states of the same spin and parity. If the wave function of Eq. (4) is now taken to represent one of these T = 1/2 states, i.e. a is small, then a^2 is a measure of the T = 3/2 admixture in that state. If it is possible to estimate or measure a, (which implies an estimate of or knowledge of b), second order perturbation theory yields the following charge-dependent matrix element:

$$\langle T = 3/2,\ T_z = -1/2 | H_c | 1/2,\ -1/2 \rangle = (E_{3/2} - E_{1/2})\, a \quad . \tag{11}$$

Here E_T is the energy of the state of predominant isospin T and H_c contains the Coulomb potential and any other charge-dependent terms. Thus, if evidence for the amount of T = 3/2 admixture into T = 1/2 states can be

obtained, the magnitude of charge-dependent matrix elements will then be available for comparison with future theoretical calculations.

B. First-Forbidden Beta-Decay

All of the nuclei studied have a sizeable number of allowed decay branches, so that ordinarily any first-forbidden branches could be neglected. However, ^{17}Ne arises as a special case. The first decay branch with an ft-value in the usual allowed range is that to the state at 4.609 MeV in ^{17}F. The ground and first-excited state are fed by first-forbidden transitions, the fourth excited state is fed by a second-forbidden transition, and the third excited state is fed by an allowed transition which is strongly inhibited due to cancellations in the relevant ^{17}F wave function.[37] The strong energy dependence of beta-decay made it necessary to determine the intensity of the weak first-forbidden branches in this case.

The two ^{17}F states involved are proton stable and are not characterized by proton emission, unlike the third and higher excited states. Unfortunately it is not correct to assume that the ft-values for these transitions are identical to those for the mirror decays[38] from ^{17}N, since the shape of the β-particle energy spectrum differs from that for allowed decay.

The generalized statistical rate function is[39]

$$f_n = \int_1^{W_o} p_e W_e (W_o - W_e)^2 \, F(Z, W_e) \, C_n \, dW_e \quad , \tag{12}$$

where n is the order of forbiddenness; W_o is the total decay energy in units of mc^2; p_e and W_e are the momentum and energy of the beta-particle,

respectively; $F(Z, W_e)$ is the Fermi function that takes account of the effects of the nuclear charge and C_n is the appropriate shape factor. For allowed decay C_o is a constant but for first-forbidden decay[39]

$$C_1(W_e) \propto 1 + aW_e + b/W_e + cW_e^2 \quad , \tag{13}$$

where a, b, and c depend on six nuclear matrix elements in a complicated way. For unique first-forbidden transitions ($\Delta J = 2$) five of the matrix elements vanish and $b = 0$. The ratio f_1/f_o for this case has been calculated[40] as a function of Z and W_o, as the only remaining matrix element factors out. Since the ground state transition ($1/2^- \longrightarrow 5/2^+$) in mass 17 is first-forbidden unique, the intensity of this branch was calculated by assuming $\underline{f_1 t}$ to be identical for both β^-- and β^+-decay.

The decay of ^{17}Ne to the first excited state of ^{17}F, ($1/2^- \longrightarrow 1/2^+$), involves five of the six possible matrix elements and in the absence of model calculations the exact relationship of the mirror decays cannot be determined. For the purpose of analysis, an <u>ft</u>-value midway between those determined by using C_o and C_1 (unique) was assumed. In view of the uncertainty in this procedure, error bars which overlapped both values were assigned. An unusual amount of coherence among the matrix elements would be required to cause this error to be exceeded.

C. Induced Tensor Coupling in Beta-Decay?

The <u>ft</u>-values for the mirror β-decays, $^{12}B \xrightarrow{\beta^-} {}^{12}C$ (g.s.) and $^{12}N \xrightarrow{\beta^+} {}^{12}C$ (g.s.), are not identical. A detailed calculation of radiative and other effects failed to explain the observed asymmetry.[1] In order

to explain this phenomenon, it has been suggested that an induced tensor term contributes to nuclear β-decay.[2,3] Since the induced terms are generally neglected a sketch of their origin is given below. Further details are available in the references cited.

By analogy with electromagnetism, nuclear beta-decay is often considered to result from two currents interacting with each other, the nucleon (or hadronic) current and the lepton current. The product of these currents describes the interaction and yields a Hamiltonian density,

$$\mathcal{H} = \frac{G}{\sqrt{2}} \overline{\psi}_N \, H \, \psi_N + \text{H.c.} \tag{14}$$

where G is a coupling constant. The first term of Eq. (14) gives rise to β^--decay while its Hermitian conjugate (H.c.) produces β^+-decay. In the absence of strong interactions, the universal vector-axial vector interaction says the operator H will have the form[41]

$$H_{\text{"bare"}} = \gamma_\mu (1 + \gamma_5) \, L_\mu \quad , \tag{15}$$

where L_μ is the lepton current,

$$L_\mu = \overline{\psi}_e \, \gamma_\mu (1 + \gamma_5) \, \psi_\nu \quad . \tag{16}$$

The γ_μ and γ_5 are the usual Dirac operators. When the strong interactions are switched on H becomes[42]

$$H + [\gamma_\mu (1 + \lambda \, \gamma_5) + i \, \sigma_{\mu\nu} (A + B \, \gamma_5)^{\partial}/\partial\chi_\nu + (C + D \, \gamma_5)^{\partial}/\partial\chi_\nu] \, L_\mu \quad , \tag{17}$$

where A, B, C, and D are form factors and λ is the ratio g_A/g_V. Time reversal invariance requires the form factors to be real.

Conserved vector current (CVC) theory deals with the coefficients 1, A and C, predicting the magnitude of A--the "weak magnetism" term--and the disappearance of C. It has met with considerable success in explaining experimental results, such as the β-spectrum shape for the decays of ^{12}N and ^{12}B, and is generally accepted. The theoretical situation with regard to the other terms in Eq. (17) is not so clear. Partial conservation of the axial vector current (PCAC) predicts the magnitude of λ and D but does not say anything about B, the induced tensor term.[43] PCAC's prediction for D is essentially identical to a prediction[44] based upon dispersion theory which gave

$$D/\lambda \approx -0.04 \quad , \tag{18}$$

lending support to PCAC theory. Such a weak component is virtually undetectable in β-decay although μ-capture measurements indicate this estimate has the correct order of magnitude (see Ref. 43).

The transformation G is defined as

$$G \equiv C\, e^{i\pi T_2} \quad , \tag{19}$$

where C is the charge conjugation operator which changes a particle into its antiparticle. The other factor rotates the isobaric spin vector by 180° about the 2-axis. Since strong interactions are charge symmetric and charge conjugation invariant, they are invariant under G also. This property allows the terms of Eq. (17) to be split into two groups according

to their properties under G transformation.[42] If weak interactions are assumed to be invariant under G then the "second-class" terms, B and C, must vanish. CVC has already eliminated C for other reasons so B is the logical place to look for a second-class current.

When account is taken of all terms possibly comparable to those caused by B, the ratio of mirror beta decays, assuming identical Gamow-Teller matrix elements, is given by

$$(\underline{ft})^+/(\underline{ft})^- = (1 + C_1^- + A\,C_2^- + B\,C_3^- + D\,C_4^-)/(1 + C_1^+ + A\,C_2^+ + B\,C_3^+ + D\,C_4^+), \quad (20)$$

where C_1, C_2, C_3, and C_4 are complicated functions depending on various matrix elements and the energies involved. For small corrections Eq. (20) can be written as

$$\delta \equiv (\underline{ft})^+/(\underline{ft})^- -1 = (C_1^- - C_1^+) + A(C_2^- - C_2^+) + B(C_3^- - C_3^+) + D(C_4^- - C_4^+) \ . \quad (21)$$

It is clear from Eq. (21) that only those terms that change sign in going from β^-- to β^+-decay will contribute significantly. Portions of the C_1, C_3, and C_4 terms do this. However, C_4 contains[4] a 1/M factor, where M is the nuclear mass, thus making the contribution due to D negligible as mentioned previously. The C_1 term is quite complex and the difference $(C_1^- - C_1^+)$ is also expected to be quite small. Therefore the deviation from mirror symmetry is given approximately by[4]

$$\delta \approx 4/3 \left|\frac{g_V}{g_A}\right| B(W_o^+ + W_o^-) \quad , \quad (22)$$

where $W_o^2 >> 1$ and $(\alpha Z)^2 << 1$, both suitable assumptions for light nuclei, and B represents the strength of the induced tensor coupling.

Table II[45-60] lists values of δ and $(W_o^+ + W_o^-)$ for all mirror pairs for which sufficient information is presently available to test this relation. It is unlikely that there will be many immediate additions to this list. Of the known T = 1 mirror pairs not listed, only the β-decay of the A = 24 metastable state was excluded due to a lack of experimental data. Masses 26, 34, 38, and 42 were excluded because they undergo pure Fermi decay ($0^+ \longrightarrow 0^+$), masses 14 and 32 because their quite high ft-values indicate extreme sensitivity to slight variations in the wave functions, and masses 22, 36, and 40 because the mirror decay is first- (or greater) forbidden. The situation is slightly better for T = 3/2 pairs since improved experimental data would allow analyses of masses 33 and 37. Mass 41, however, is not a useful case since the decay of ^{41}Ca is first-forbidden. Thus, with but three exceptions, additions to the table require the discovery and characterization of unknown nuclei.

Before proceeding to use the data of Table II and Eq. (22) to extract a value for B, it is necessary to consider any other effects which may cause a nonzero δ. For the case of mass 12, Blin-Stoyle and Rosina have considered[1] many possible corrections including electromagnetic effects, second-forbidden effects, isospin mixing, and binding energy effects. All of them were unable to explain the observed deviation from mirror symmetry.

Unfortunately many of these corrections depend on the wave functions involved. In particular, determination of the binding energy effect, which

Table II. A comparison of mirror beta-decay rates.[a]

A	Parent nucleus	Final state(MeV)	E_{max}(MeV ± keV)[b]	Half-life	Branch(%)	$[W_o^+ + W_o^-](mc^2)$[c]	δ[d]
8	^{8}B	3.0	17.052±2	774±4 ms	e	51.6	0.113±0.008
	^{8}Li		16.097±2	850±4 ms(7)			
9	^{9}C	f(45)	15.469±3(22,46)	126.5±0.9 ms(21,22,g)	f	55.3	$0.179^{+0.100}_{-0.022}$
	^{9}Li		13.614±20	175.7±0.9 ms(45,47)			
12	^{12}N	0	16.320±5	10.97±0.04 ms(8)	94.3±0.5(8)	60.1	0.103±0.009
	^{12}B		13.370±1	20.41±0.06 ms(8)	97.1±0.3(8)		
13	^{13}O	h(48)	16.738±10(46,49)	8.9±0.2 ms(23,g)	h	59.5	0.15±0.03
	^{13}B		13.437±4	17.33±0.17 ms(50)			
17	^{17}Ne	i	13.534±23(49)	109±1 ms(g)	i	24.9	0.148±0.024
	^{17}N		8.679±15	4.16±0.01 sec(10)			
18	^{18}Ne	0	3.425±5	1.674±0.018 sec(51,52)	92.4±1.7	5.5(j)	-0.003±0.015
	^{18}F		0.633±1	109.87±0.12 min	97.0±0.2		

(continued)

Table II (continued)

A	Parent nucleus	Final state(MeV)	E_{max}(MeV ± keV)[b]	Half-life	Branch(%)	$[W_o^+ + W_o^-](mc^2)$[c]	δ[d]
20	^{20}Na	1.63	12.89±40	451±2 ms(15)	k	34.6	0.062±0.031
	^{20}F		7.030±5	11.03±0.06 sec(53)	99.98		
21	^{21}Mg	k	12.070±17	121±5 ms(26)	k(28)	35.1	0.75±0.37
	^{21}F		5.684±7	4.32±0.04 sec(54)	k(55)		
24	^{24}Al	4.12	12.862±7	2.081±0.009 sec(16)	8.0±0.5	21.8	-0.03±0.06
	^{24}Na		5.515±3	14.981±0.011 h	99.92±0.02		
25	^{25}Si	k	11.688±42(49)	218±4 ms	k(29)	29.5	0.187±0.076
	^{25}Na		3.835±9	59.6±0.7 sec	k(56)		
28	^{28}P	1.78	13.316±9	270.3±0.5 ms	52±2	30.2	0.25±0.05
	^{28}Al		4.635±4	2.246±0.004 min(57)	100		
29	^{29}S	k	12.795±35(49)	189±7 ms(25,30)	k(28)	28.0	0.29±0.16
	^{29}Al		3.676±7	6.52±0.05 min(58)	k(56,59)		
30	^{30}S	0	5.115±12(60)	1.27±0.02 sec(m)	20±1	3.7(j)	0.02±0.05
	^{30}P		3.217±6(60)	2.497±0.005 min	99.5±0.1		

(continued)

Table II (continued)

[a]This table is an updated version of a similar table in Ref. 3. The references cited here represent additions or corrections to the earlier table.

[b]E_{max} is the maximum β-particle energy for the ground state transition.

[c]$(W_o^+ + W_o^-)$ is the weighted average if more than one final state is involved in the comparison.

[d]Values of f were calculated using the method given by J. N. Bachall in Nucl. Phys. 75, 10 (1966).

[e]Integration was carried out over the entire range of ^{8}Be excitation. See Ref. 3.

[f]The decay rate of ^{9}C was computed using the known[45] rates for ^{9}Li decay. The upper limit is derived from theoretical predictions for unobserved branches. See Ref. 3.

[g]Present work.

[h]The half-life of ^{13}O was predicted from the ft-values known[48] from the mirror decay, taking into account the additional branches to high lying states of ^{13}N observed in this work, and the result was compared with the experimental value.

[i]The strengths of the first-forbidden decays of ^{17}Ne to the two lowest states of ^{17}F were calculated using ft-values from the mirror decays. Then the decays to the remaining states were compared.

[j]Since both nuclei are positron emitters, this entry is the difference of the decay energies.

[k]The strength of the superallowed β^+-decay branch was calculated assuming complete isobaric-spin purity. This was used in conjunction with delayed-particle data to calculate the partial half-life for β^+-decay to all the particle-emitting states. The decay rate to the remaining state (or states) was then compared to that of the

(continued)

Table II (continued)

mirror β^--decaying nucleus.

[m]This lifetime was calculated assuming an ft of 3120 sec for the superallowed transition and using the known branching ratios. See Ref. 3.

results from the distortion of identical single-particle states caused by the Coulomb potential, requires knowledge of the wave functions. The most recent calculation[61] of this effect for mass 12, which also took account of relativity, predicted a δ ranging from 0.012 to 0.037, considerably less than the experimental value. The initial study[1] of mass 12 showed this correction to be the dominant one.

This correction is not available for the other cases listed in Table II. Therefore, it was decided to neglect the two small corrections with only minor dependence on the wave function: the effect of finite nuclear size and those radiative effects that do not simply renormalize the vector and axial vector coupling constants. The latter, "outer" radiative effects are tabulated[62] and have the same sign for β^+- and β^--decay. They therefore tend to cancel out. For example, this correction would reduce δ in the case of ^{17}Ne by 0.003. The approximate effects of finite nuclear size are available[63] in graphical form and except for low Z and high W_o have opposite signs for β^+- and β^--decay. For the case of mass 20 this correction increases δ by about 0.013. These examples, plus the observation that the binding energy effect and the finite nuclear size effect have opposite signs, justify the neglect of these corrections. In addition the errors on most values of δ listed in Table II are considerably larger than the corrections.

Figure 1 shows a plot of δ versus $(W_o^+ + W_o^-)$ and a least-squares fit to the data, similar to that in Ref. 3. The line was required to go through the origin. The mass-21 data have not been used due to the large error bar on δ. Use of Eq. (22) then gives

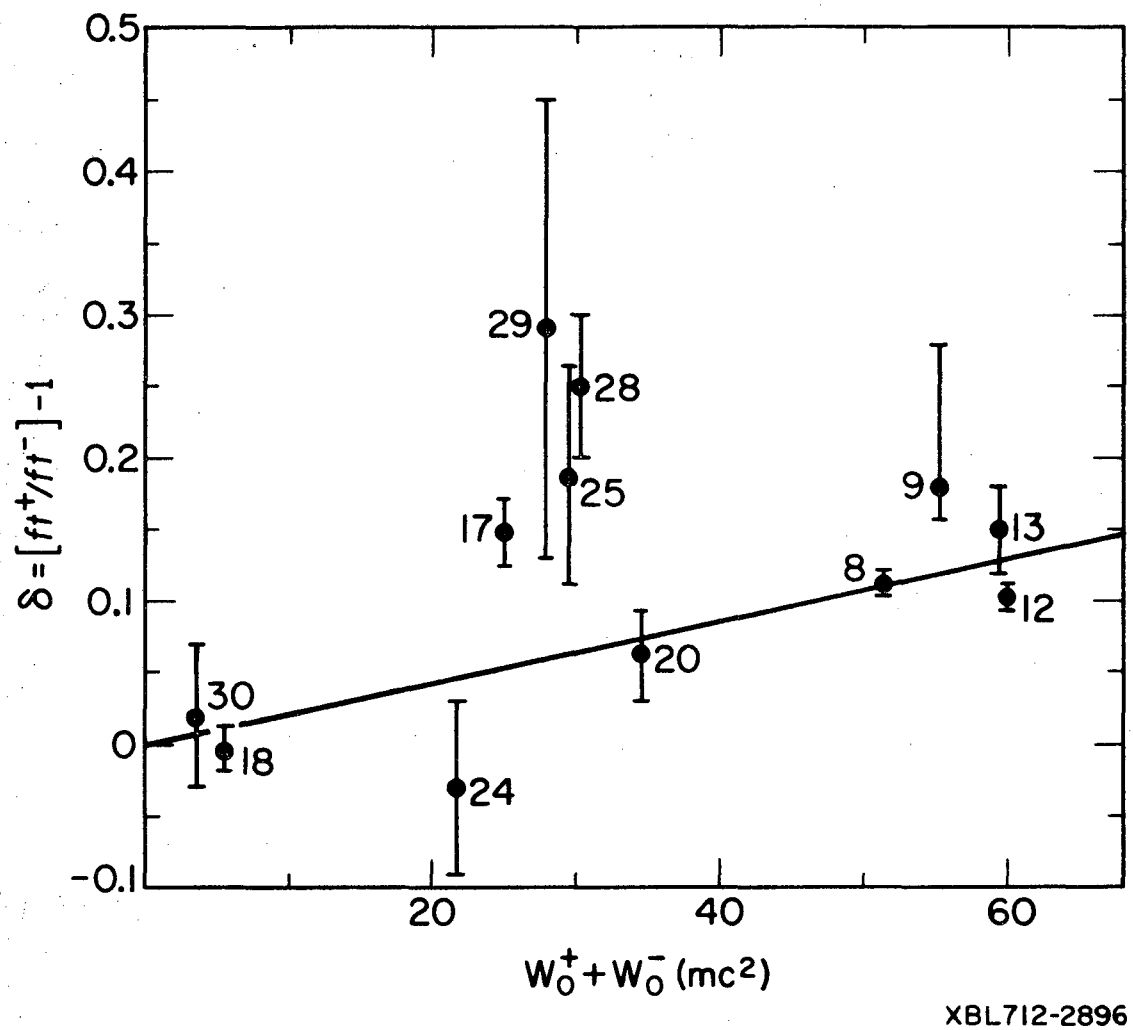

Fig. 1. A plot of deviations from mirror symmetry in β-decay versus the total decay energies. The line is a weighted least-squares fit to the data. The data points are labeled with the mass of the mirror pair.

$$B \sim 2 \times 10^{-3} \quad . \tag{23}$$

However, it has been suggested[64] that an equivalent form of Eq. (17) can be written that leads to a change in Eq. (22) such that B should be larger by a factor of two. However if some assumptions are made about meson exchange effects this difference is essentially eliminated.[64] Since the main thrust of this analysis is to determine whether or not the induced tensor term B exists, such differences are not too important at this stage.

In this connection, a recent paper[65] states that none of the one-body operators in Eq. (17) can produce mirror asymmetries in decay rates. The paper also states that multinucleon or meson-exchange effects cause the observed asymmetry. As mentioned above, however, certain meson-exchange effects result in an <u>effective</u> one body operator that has the same form as an induced-tensor interaction and is of many body origin.[64] Thus the study of mirror asymmetries may eventually yield information relevant to the existence of both second class currents and meson exchange effects.

As can be seen from Fig. 1, the data for odd-mass nuclei lie above the line and the opposite is true for the even-mass nuclei; only two exceptions are noticeable. This apparent trend and the substantial scatter of points indicate that, although whatever is causing deviations from mirror symmetry seems to increase as $(W_o^+ + W_o^-)$ increases, there are still some unexplained effects present. One possible explanation for the high values of δ for odd-mass nuclei heavier than mass 17 would be the presence of significant isospin impurity in the lowest T = 3/2 analogue state in the

$T_z = -1/2$ nuclei. The analysis of the data for these nuclei required the assumption of pure isobaric spin for the analogue states. If some amount of isospin impurity were assumed, the value obtained for δ would decrease. As will be apparent later there is substantial evidence for an impurity of about 10% in the T = 3/2 state of ^{33}Cl. Good calculations of the binding energy effects might also help reduce the large scatter of the points.

III. EXPERIMENTAL METHODS

A. Cyclotron and Beam Transport

All the experiments were performed in the Cave 2 external beam facility of the 88-inch cyclotron. The beam transport system has been described[66] in detail previously. Since only the reaction products were of interest, the beam optics were adjusted for maximum beam transmission, with the constraint that the beam be focussed sufficiently to avoid hitting the target holder or scattering chamber. This method tends to produce a larger beam spot, permitting higher beam intensities without burning out the target. For both proton and ^{3}He bombardments, typical beam currents on target were about 3 μA, limited in most cases by subjective estimates of the potential lifetime of the target or isolation foil.

B. The Pulsed-Beam, Shielded-Detector Method

The main experimental difficulties in the study of delayed-proton emitters arise as a result of the fairly low cross sections for their formation. In order to achieve reasonable counting rates, it is necessary to use high beam intensities and good geometries. This requirement, along with the fact that relatively high energy beams ($\sim$ 35 MeV for ^{3}He's and $\sim$ 45 MeV for protons) are needed, causes the two major problems: radiation damage of the detectors and enormous amounts of β- and γ-background radiation. A great deal of experimental effort has been directed at minimizing these two difficulties. An approach which consisted of providing better detector shielding produced improved spectra. This system was used to investigate some (^{3}He,2n) cross sections for light nuclei.

The earliest work on delayed-proton emitters used a pulsed beam and a single detector that viewed the target continuously.[24] The scattered beam produced radiation damage in the detector, resulting in rapid progressive deterioration of the energy resolution during the experiment. Use of a single counter also resulted in high backgrounds at low energies, $\lesssim 3$ MeV, due to multiply-scattered β-particles.

Preliminary work attempted to deal with the latter difficulty. A counter telescope consisting of a thin transmission ΔE detector followed by a thick E detector was used. A fast coincidence requirement between the two detectors eliminated most of the β-particle induced background. In addition use of two detectors permitted the application of particle identification techniques (see Sec. III D) which further reduced the background.

However the problem of radiation damage remained, resulting in detector lifetimes shorter than the planned duration of the experiments. The preliminary experiments also uncovered another potential difficulty. About once every few hours the beam pulsing system would fail and the beam would continue into the counting period, effectively eliminating all data accumulated up to that point. The cause of this problem is not known, but may be due in part to elements of the cyclotron radiofrequency system that automatically produce recovery from tank sparks.

In order to deal with these difficulties, the apparatus shown in Fig. 2 was constructed. A remotely controlled rotating wheel of 3.2 mm tantalum shielded the detectors during the beam-on periods. Provision was made for the simultaneous use of two counter telescopes, at angles of 35.5°

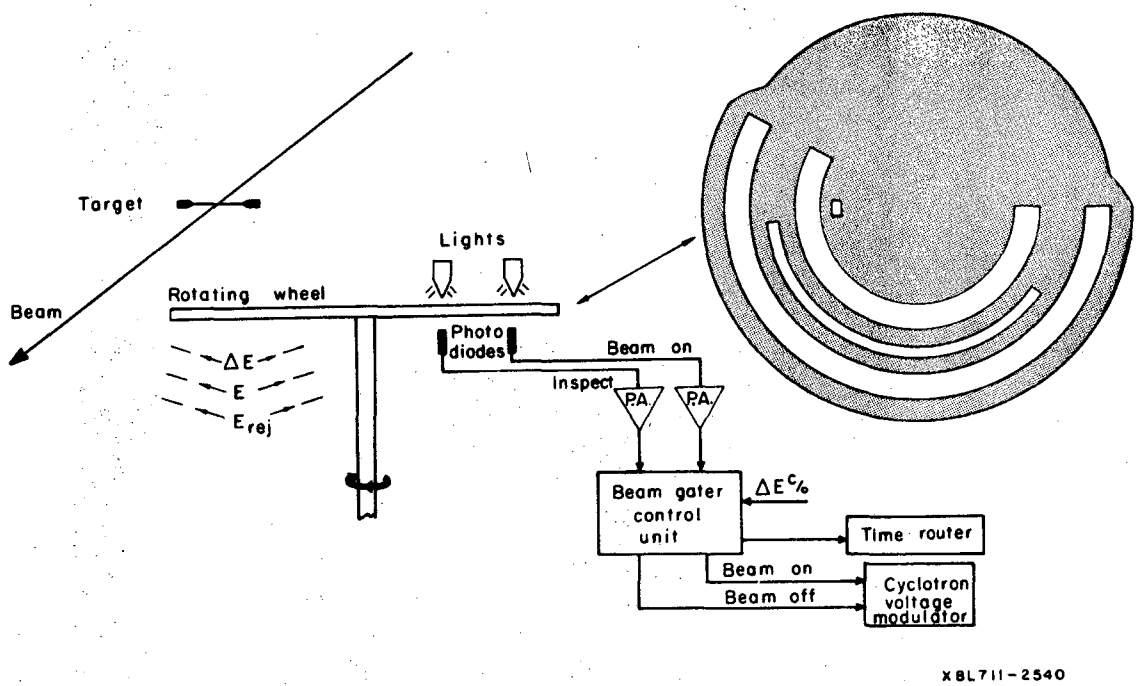

Fig. 2. A diagram of the beam-shielding apparatus used in the pulsed-beam, shielded-detector method.

and 70.5° to the beam. During counting periods the detectors could view the target through the large slots in the wheel. The thin slots and the two light-photodiode pairs provided positive control of the beam pulses and provided protection against failure of the beam-pulsing system.

Beam pulsing was controlled by the rightmost photodiode in Fig. 2. When this photodiode received light, the beam was turned on. When the wheel rotation shielded this photodiode from the light, the cyclotron dee voltage was reduced by about 20 kV from the usual value of 40 to 50 kV. Experiments with the wheel stopped in the "beam on" position proved that this change was sufficiently drastic to completely eliminate the beam.

The "inspect" pulse generated by the other photodiode provided protection against the occasional failures of the beam pulsing arrangement. While the inspect pulse was present, circuits in the beam gater control unit compared the count rate in one of the detectors, usually the forward angle ΔE, to a preset level. If this level was exceeded, the pulse which started the time router was not generated and the data were not stored. (See Sec. III D for details of the electronics.)

This arrangement was used to study the delayed-proton emitters ^{17}Ne, ^{21}Mg, ^{25}Si, and ^{41}Ti. The (^{3}He,2n) reaction on $\sim$ 700 μg foils of magnesium and calcium was used to produce ^{25}Si and ^{41}Ti, respectively. The foils were rotated 60° toward the detection systems to increase the effective target thickness. The nuclei ^{17}Ne and ^{21}Mg were produced by the $^{16}O(^{3}He,2n)^{17}Ne$ reaction and the $^{20}Ne(^{3}He,2n)^{21}Mg$ reaction, respectively. The target for these reactions consisted of about 0.5 atm of the appropriate gas in a 5 cm long cylindrical gas cell with 2.5 μm Havar windows. The

density of the gas target was fairly low so the bulk of the product nuclei lodged in the exit foil which was tilted 52.5° toward the detectors. With this geometry only those decays occuring within the foil or within a relatively small volume of gas immediately behind the foil could be observed.

The spectra obtained for these four nuclei were marginally better than those obtained previously, but not sufficiently so as to yield appreciable new results. However these experiments did provide some cross section measurements for the (^{3}He,2n) reaction on light nuclei. The only previous cross section datum for production of delayed-proton precursors via ^{3}He induced reactions was an excitation function[27] for ^{17}Ne that only extended to 5 MeV above threshold. The results of these cross section measurements, which took into account the loss of activity due to recoil[67] out of the target, are listed in Table III. The method of computing the cross section is described in Appendix A. Due to the thick targets, some of the beam was scattered enough to miss the Faraday cup. While experimental measurements of this effect were made, the possibility of variations in the beam optics during an experiment results in errors of about 50% on the absolute cross sections. The relative errors for a single target are undoubtedly better. The 31 MeV datum for ^{17}Ne is in agreement with the previous result.[27] Figure 3 shows an excitation function for the ^{24}Mg(^{3}He,2n)^{25}Si reaction. It is noteworthy that the cross section decreases quite slowly with increasing energy.

Table III. Some cross sections for (^{3}He,2n) reactions.

Product nucleus	Beam energy (MeV)	Cross section[a] (μb)
^{17}Ne	31	36
	80	5.6
^{21}Mg	31	230
	80	66
^{25}Si	32	120
	38	150
	43	140
	60	130
^{41}Ti	40	27

[a]The absolute error is about ±50%.

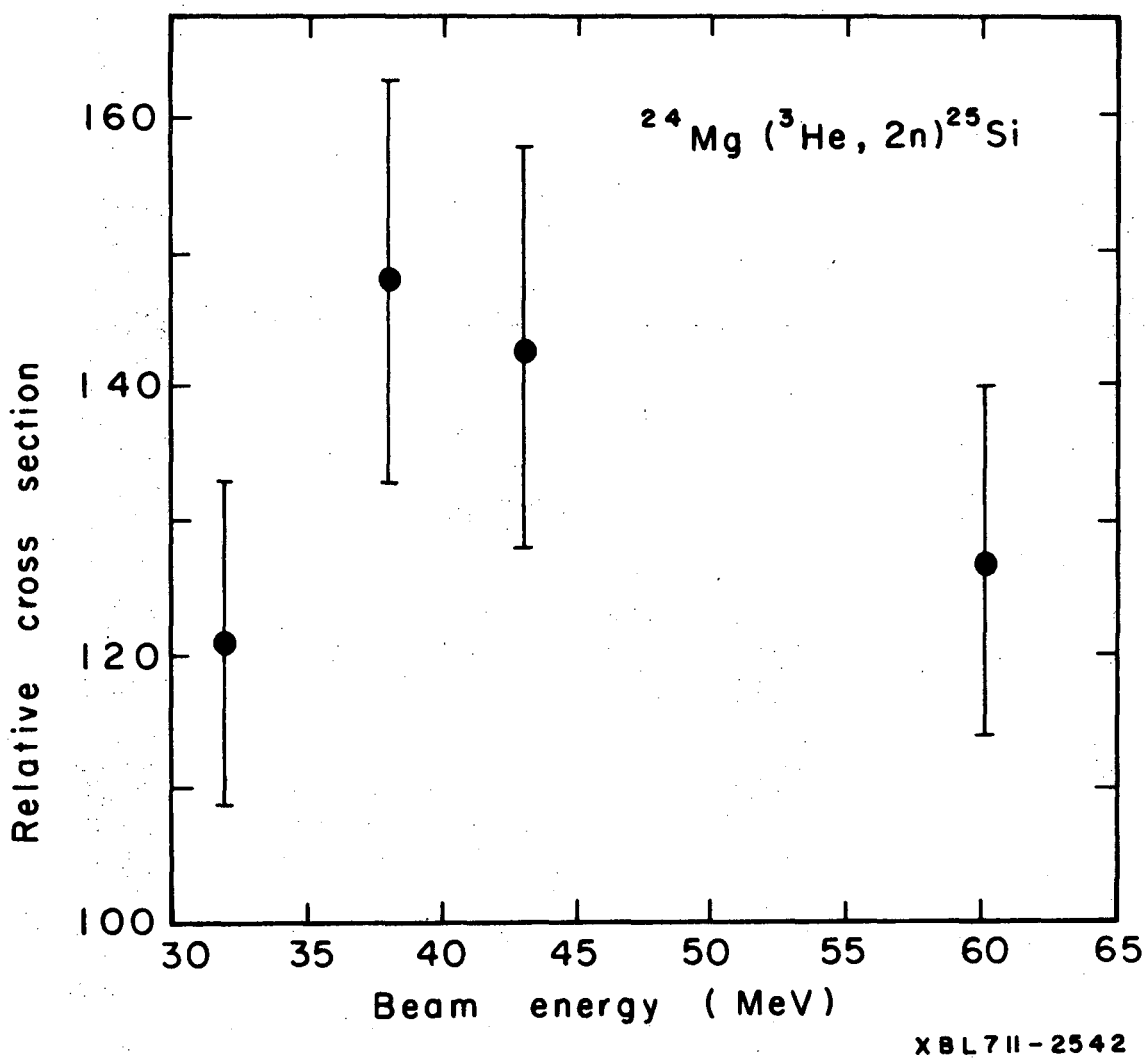

Fig. 3. A relative excitation function for the $^{24}Mg(^{3}He,2n)^{25}Si$ reaction. The ordinate is approximately the absolute cross section in μbarns.

C. Gas-Sweeping System

The pulsed-beam, shielded-detector method did improve the life expectancy of the detectors, but it failed to produce radically improved spectra. Two possible causes for this failure come to mind. First, the buildup of background β- and γ-activities in the target may cause poor resolution due to pileup or other processes. Second, the proton emitters are distributed throughout some part of the target (or exit foil) and therefore the emitted protons will exhibit an energy spread proportional to the target thickness.

A system for gaseous activities that avoids the problems discussed above was constructed. (However, both solid and gaseous targets can be used.) The activity of interest is swept from the target area by a blast of some carrier gas to a distant well-shielded counting chamber. The resultant diffuse source is virtually weightless. The γ- and β-backgrounds are considerably reduced due to the shielding. Also, only gaseous products should arrive in the counting chamber, which is evacuated at one point in each counting-bombardment cycle. This prevents the gradual buildup of long-lived background activities.

Figure 4 shows the apparatus used for the study of ^{33}Ar ($\tau_{1/2}$ = 173 ms) produced via the $^{32}S(^{3}He,2n)^{33}Ar$ reaction. The study of other nuclei required various modifications but the basic principles remained the same.

The 20 cc, 10 cm long target chamber was filled when valve 1' operated. The target windows were 2.5 μm Havar foils. The 1.5 liter CS_2 reservoir was heated to about 30°C by an electric mantle. Under the

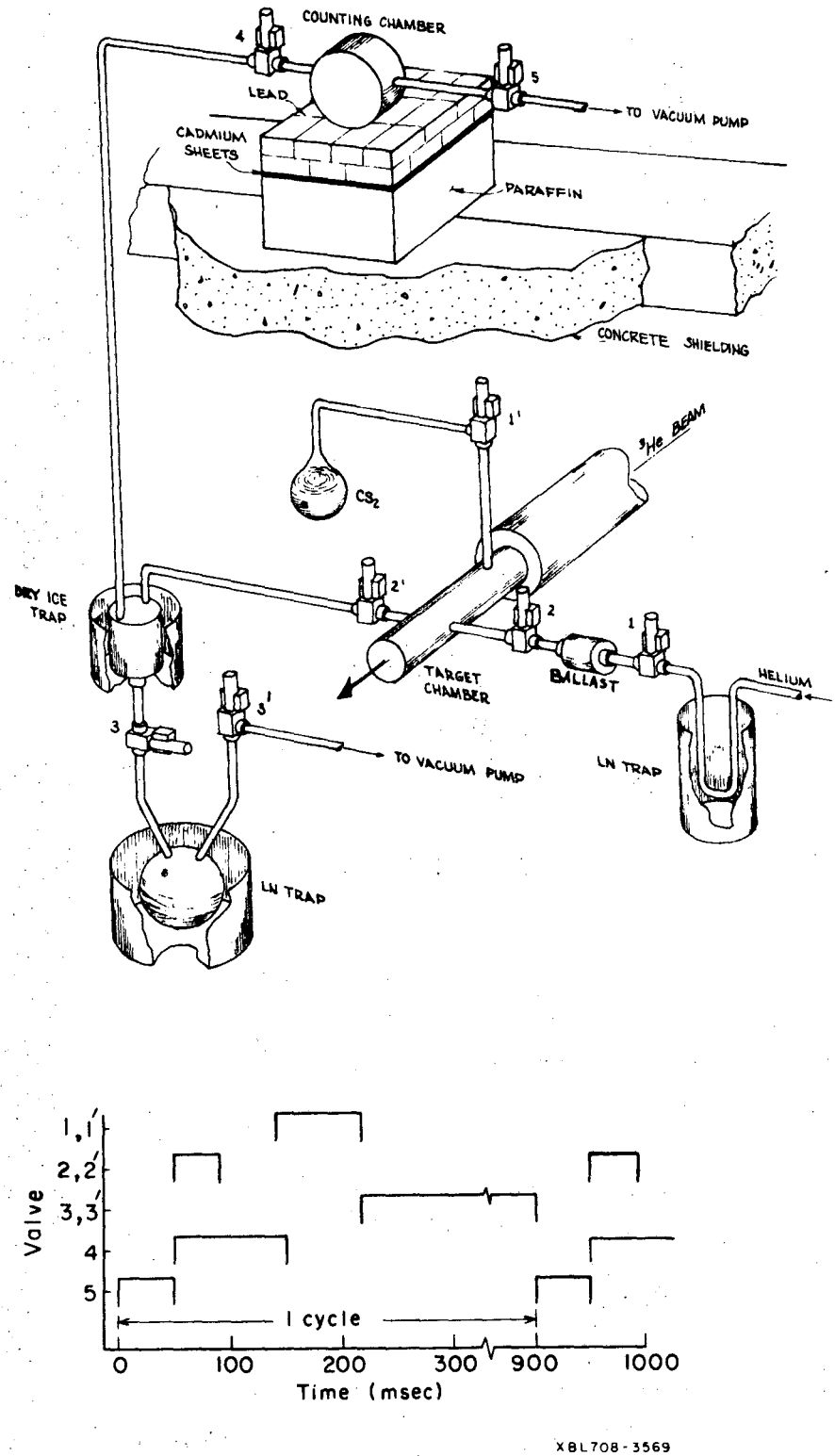

Fig. 4. A diagram of the gas-sweeping system used for the production of ^{33}Ar via the ^{32}S(^{3}He,2n)^{33}Ar reaction. The diagram at the bottom shows the sequence of valve operation and typical "valve-on" times.

conditions generally used, a single filling lasted about twelve hours. While the target filled, valve 1 allowed helium to flow into a variable-volume ballast chamber. The liquid nitrogen trap removed any condensable impurities in the helium and also prechilled the gas. The yield improved as the ballast volume was decreased to its minimum size of $\sim$ 10 cc while the pressure was increased correspondingly to 1.5 atm. The product of volume and pressure allowable was determined by the capacity of the vacuum system.

When valves 2 and 2' opened, the high pressure helium swept the CS_2 vapor and the argon activity through a 60 cc dry ice-trichlorethane trap that removed about 80% of the CS_2 from the gas stream. The gas then passed through a small glass wool trap which removed particulate sulfur formed by radiation decomposition of CS_2. Finally the gas flowed via 6.4 mm i.d. teflon tubing to a shielded counting chamber about 5 meters from the target. The total transit time was about 100 ms. At this point, valve 4 closed and counting began. The "waste" gas left in the line was then removed by opening valves 3 and 3'. The LN trap prevented contamination of the pump oil with CS_2. After counting was complete, valve 5 opened and the counting chamber was evacuated. The diagram at the base of Fig. 4 shows typical durations and the order of valve operation.

Figure 5 shows the counting chamber used. The bulk of the chamber is aluminum, with stainless steel used as a standoff for the copper cold-finger. The spacer, indicated by the diagonal lines, was made of laminated fiberglass to reduce heat conduction from the chamber walls. Liquid nitrogen was used as a coolant to provide the high cooling capacity required by the high gas flow rate. The gas inlet and outlet were both located at

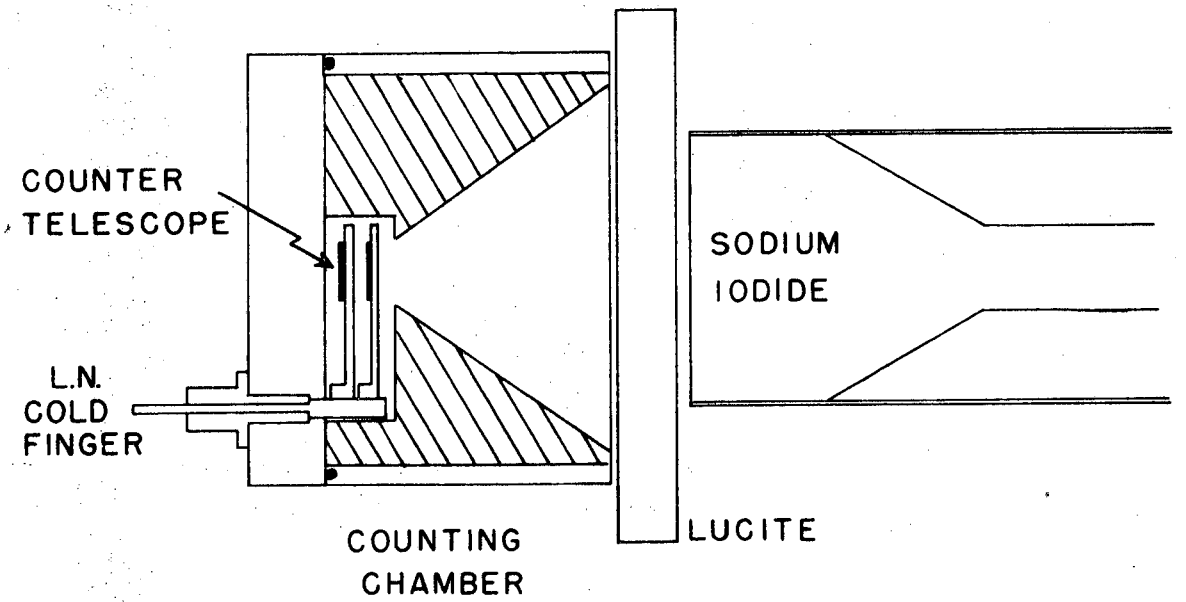

Fig. 5. A schematic diagram of the counting chamber used for the study of gaseous, delayed-proton emitting sources.

the base of the conical gas volume. A transducer was also mounted at the base to permit continuous monitoring of the shape and magnitude of the gas pulses. The end wall of the chamber was only 0.8 mm thick, to reduce attenuation of γ-rays. This problem was not too severe since it was not necessary to look for any γ-rays below 511 keV.

The use of CS_2 as a target was a distinct advantage in this case, as it is unlikely that a solid sulfur target could have withstood the 3 μA ^{3}He beams used for extended periods of time. However solid targets were used for some other nuclei. The delayed-proton emitter ^{17}Ne was produced via the $^{16}O(^3He,2n)^{17}Ne$ reaction on a stack of six oxidized titanium foils. The foils were held about 0.5 mm apart to allow helium to sweep between them. In this case valve 1', the dry ice trap and assiciated LN trap, and valve 3 were no longer necessary. A small LN trap was used to remove any condensable products. The use of O_2 gas in place of the CS_2 flask in the apparatus of Fig. 4 provided an alternate means of producing ^{17}Ne. Similarly the $^{14}N(p,2n)^{13}O$ reaction on N_2 gas was used to produce ^{13}O.

Not all desired targets are available as strong foils or as gases, so an alternate technique is required. Boric acid enriched to 92.4% in ^{10}B was pressed into 100-mesh tungsten screen at 141 kg/cm^2. Five such screens were used as targets for the $^{10}B(p,2n)^9C$ reaction. In this case oxygen gas was used as the sweeper. This technique allows any solid beam-resistant material to be used as a target. Good yields were obtained for all types of targets. Noteworthy are the good results for the solid target experiments which indicate that the recoil atoms must rapidly diffuse out of the foils or granules in which they stop.

The speed of the system is limited by the speed of the valves. They take 10 to 15 ms to open, even when driven with twice their rated voltage. The length of tubing used also affects the collection time. In order to study $^{13}O(t_{1/2} = 8.95$ ms) the line length was shortened to one meter, yielding a time of 40 ms from the nominal opening of valve 2' to full pulse height. The actual transit time may be somewhat shorter, since it is not known exactly when the valves opened. The shorter length permitted less shielding which in turn led to increased background problems. A reasonable spectrum was obtained nevertheless. (See Sec. IV C.)

D. Electronics and Counting Techniques

The electronics used in conjunction with the two methods described in Secs. III B and III C were quite similar. Since the most interesting results were obtained with the latter method, the bulk of this discussion will relate to the gas-sweeping system. Areas in which the two methods used different electronics will be pointed out.

A simplified diagram of the electronics used in the gas-sweeping system is shown in Fig. 6. The circuit shown permits the simultaneous accumulation of identified proton events, p-γ coincidences, and events that correspond to particles stopping in the ΔE counter. The latter data were taken to search for the presence of low energy proton groups or alpha particles. The identified proton data were stored in up to eight sequential time groups, providing simultaneous energy and lifetime information. Signals from either the valve control unit or the time router were fed into inhibit inputs (not shown in Fig. 6) on each amplifier gate. This ensured that only data taken during desired counting periods were stored.

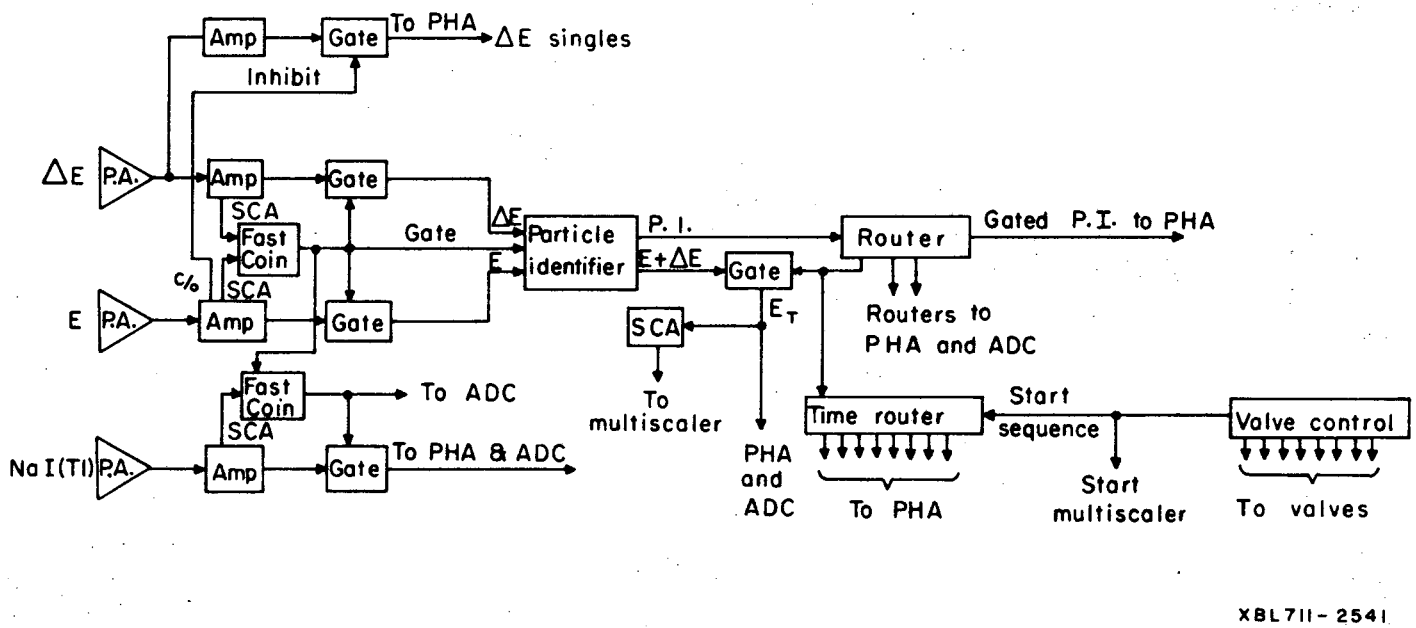

Fig. 6. A simplified diagram of the electronics used to gather singles proton, proton-γ coincidence, and ΔE singles data simultaneously.

Various counter telescopes were used to allow particle identification to be performed. They consisted of a phosphorus-diffused silicon ΔE detector ranging in thickness from 14 μm to 50 μm and a lithium-drifted silicon E counter of 0.5 mm to 1.5 mm thickness. (In the pulsed-beam, shielded detector system a 0.5 mm E_{Rej} detector was also used. If an event occurred in this detector, simultaneous events in the other detectors were not stored.) The signals from the two detectors were required to be in fast coincidence ($2\tau \approx 15$ ns) and were then fed to a Goulding-Landis particle identifier.[68] A sample particle-identifier spectrum is shown in Fig. 7. The structure labeled "β" decreases in relative magnitude as the ΔE-counter thickness is reduced. It is probably caused by multiply-scattered β-particles. Low energy electronic cutoffs could convert the expected exponential shape into something resembling a peak. Gating around the proton peak improved the resultant spectrum.

While investigating ^{13}O and the low energy proton spectrum of ^{9}C, it was necessary to use a 14 μm ΔE counter and to require the energy loss in that counter to be $\leqslant 1$ MeV. This requirement eliminated coincidences between alpha-particles and multiply-scattered beta-particles following the decay of ^{8}B (or ^{8}Li). Without this requirement the particle-identifier and energy spectra were dominated by a broad smear that, in the former case, completely obscured the proton peak. The background was identified by finding that the half-life of the particles stopping in the ΔE detector was about 800 ms, consistent with the half-lives of either or both ^{8}B(774 ms) and ^{8}Li(850 ms).

The counters were cooled to -30°C. They operated satisfactorily in an environment where the pressure fluctuated from about 35 Torr

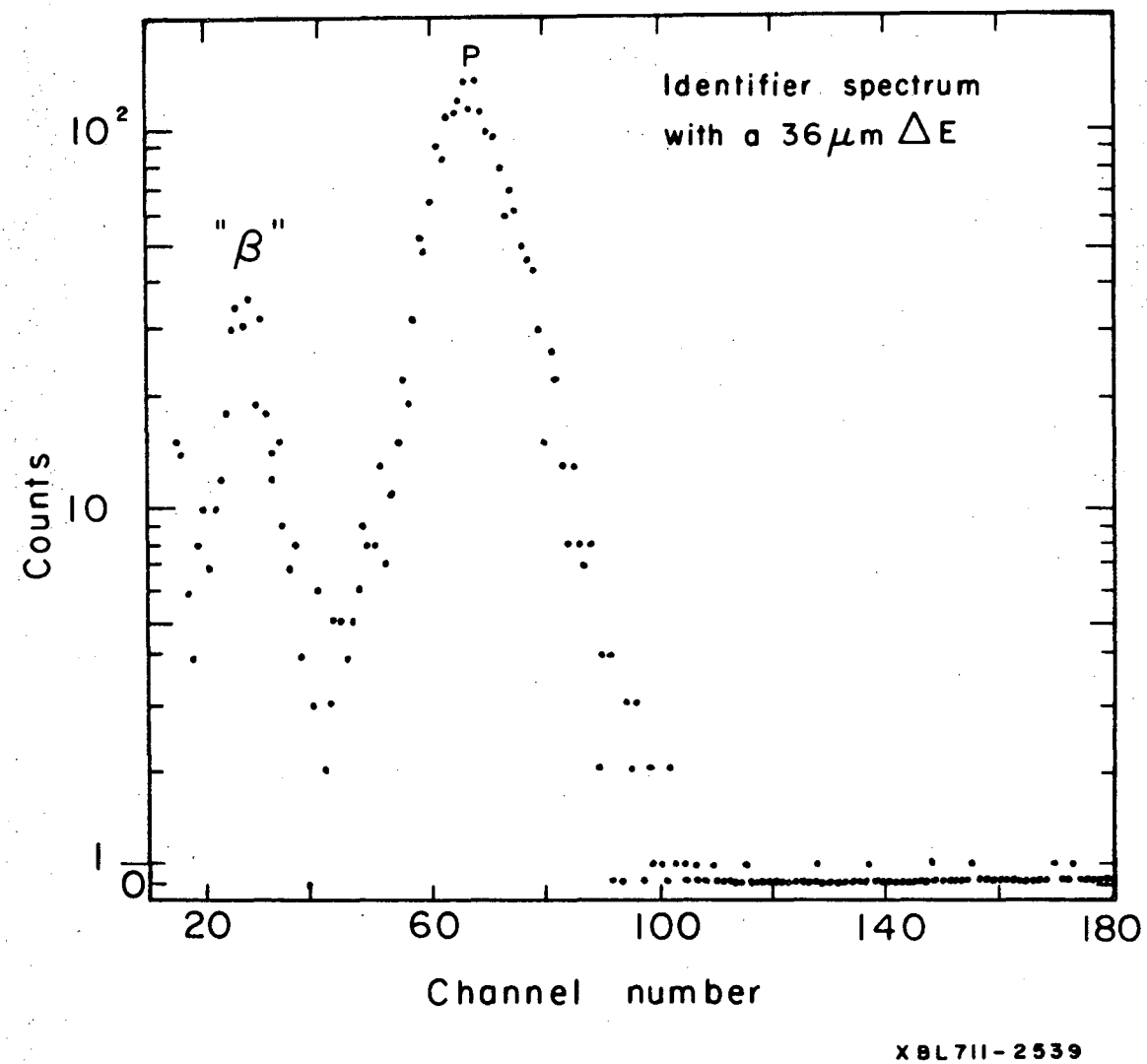

Fig. 7. A particle identifier spectrum following ^{3}He bombardment of TiO_2.

(counting) to 0.5 Torr (evacuated). No window was placed between the counters and the extended source. As a result, with a pulser resolution (full width at half maximum) of 35 keV, the observed proton peak width for narrow states was 45 keV. This additional width is due principally to the energy spread caused by the momentum of the positron. Figure 8 shows a graph of the energy spread induced by this effect for mass 33 as a function of proton and β-energy. The relevant formula is derived in Appendix 2, from which it is apparent that the effect will be even more noticeable for lighter nuclei. The relevant β-energy for use of the graph is the average β-energy for a particular transition.

Gamma-ray studies were required in the cases of ^{17}Ne and ^{33}Ar. For both nuclei a 2" × 2" NaI(Tl) crystal was used to conduct p-γ coincidence (2τ = 50 ns) measurements. The detector was placed at the base of the conical counting chamber as shown in Fig. 5. The p-γ data were recorded two-dimensionally using a PDP-5 computer.

In addition some singles γ-ray data were taken with a 45 cc Ge(Li) detector to elucidate the decay of ^{33}Ar. This detector had a resolution of ∿ 4 keV at 1 MeV, which was sufficient for these purposes. Its absolute efficiency was determined using International Atomic Energy Agency calibrated sources of ^{203}Hg, ^{22}Na, ^{54}Mn, and ^{60}Co. The efficiency curve was extended to higher energies by using the known[69] relative intensities of ^{56}Co γ-rays. The ^{56}Co source was moved from place to place within the counting chamber to allow an averaging of the efficiency over the entire active volume.

The efficiency of the counter telescope was calculated by numerical integration over the active volume and by use of a Monte Carlo program.[70]

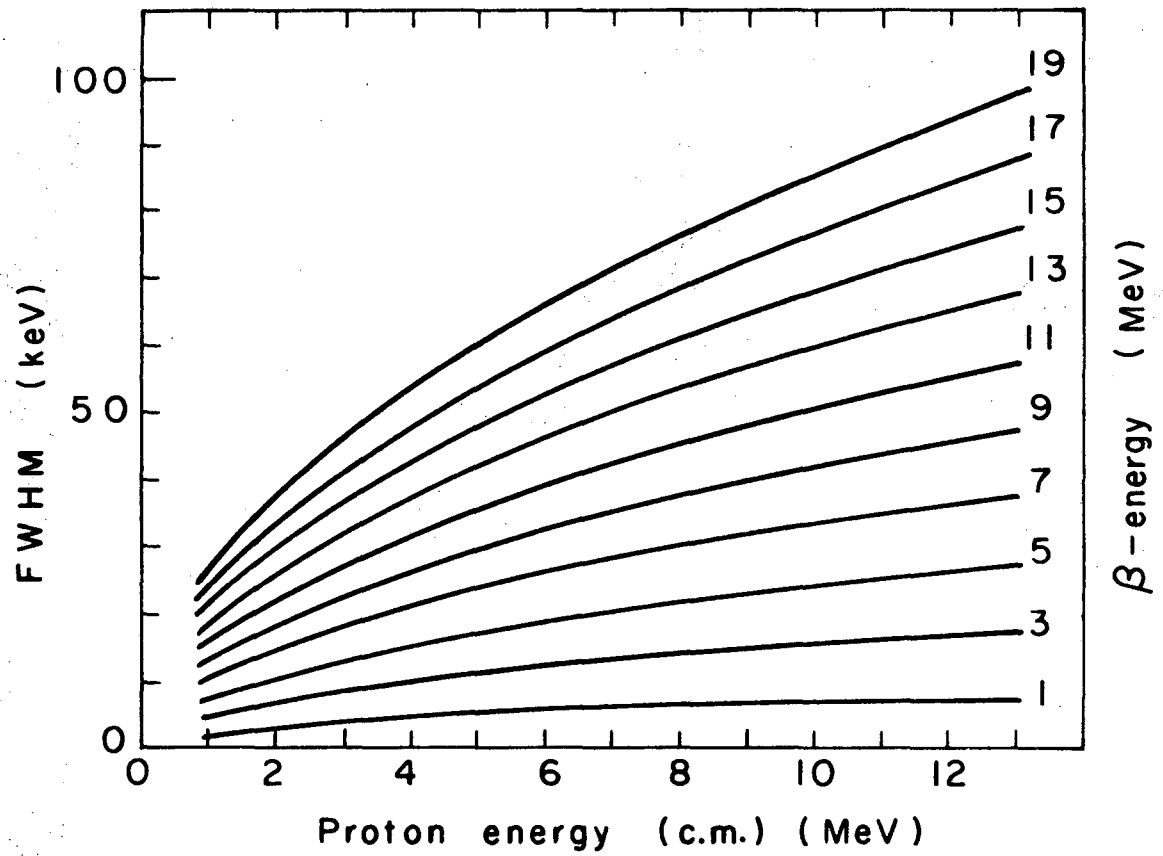

XBL711-2543

Fig. 8. A graph giving the full width at half maximum of a delayed-proton peak following the decay of ^{33}Ar under the assumption that the β-momentum is the only important contributor to the peak width. The β-energy indicated is the <u>average</u> energy for the transition of interest.

The two calculations agreed and led to a value for the efficiency of the telescope of $(1.26 \pm 0.13) \times 10^{-3}$. This arrangement was efficient enough so that about one proton per μC of beam was observed. The efficiency calculations were checked by measuring the ratio of α-particles to 388-keV γ-rays following the decay of ^{249}Cf. The ratio agreed with the measured[71] value to within 2%.

E. Half-Life Measurements

Two sources of data were used to determine half-lives: the time-sorted energy spectra mentioned previously and multiscaled data. Time-sorted energy spectra were used to check the half-lives of all observed peaks. The half-lives of all the peaks in the spectra to be shown later are consistent with the half-lives of their assigned precursors. Multiscaled data were obtained by setting gates around a selected proton peak. Events falling within these gates were stored in a 400-channel multiscaler controlled by a quartz-crystal oscillator.

The half-life data were analyzed using least squares techniques[72] and making provision for a possible longlived background. In only one case, that of ^{13}O, was such a background required. In this case, varying the background half-life from 150 ms to essentially infinity did not affect the final result. The measured half-lives using both kinds of data mentioned above were always consistent.

Averaged results for each nucleus studied are presented in Table IV, along with a comparison with earlier work. The agreement with the equally precise previous[21,22] results in the ^{9}C case is particularly gratifying.

Table IV. Half-life measurements.

Parent Nucleus	Half-life (ms)		
	Present work	Previous work	(Ref.)
^{9}C	126.5 ± 1.0	127 ± 3	(21)
		126.5 ± 2	(22)
^{13}O	8.95 ± 0.20	8.7 ± 0.4	(23)
^{17}Ne	109.0 ± 1.0	105 ± 5	(27)
		103 ± 7	(26)
		107 ± 5	(25)
^{33}Ar	173.0 ± 2.0	182 ± 5	(31)
		178 ± 10	(32)

IV. EXPERIMENTAL RESULTS

A. ^{33}Ar Decay

The delayed-proton precursor ^{33}Ar was produced by the ^{32}S(^{3}He,2n)^{33}Ar reaction on a CS_2 target. Measurements were made of the delayed protons and γ-rays which followed its decay. By identifying some peaks in the proton spectra with known levels, accurate locations for 22 levels in ^{33}Cl were obtained. Analysis of the intensities of the proton and γ-ray peaks led to ft-values for the β-transitions to 25 levels, providing information on their spin and parity. The proton groups were connected to the decay of ^{33}Ar by half-life measurements and by arguments which eliminated all possible contaminants.

Figures 9 and 10 show delayed-proton spectra produced by bombarding CS_2 with 55-MeV and 35-MeV ^{3}He beams, respectively. At 35 MeV the only known delayed-proton emitters that can be produced are ^{33}Ar, ^{32}Cl, and ^{13}O. The last has a very short half-life (∿ 9 ms) and therefore should not contribute significantly. (No trace of the known ^{13}O peaks was found.) The known[17] proton peaks following ^{32}Cl decay were not observed, nor were the ^{32}Cl delayed-alphas visible in the spectra of those events stopping in the ΔE-detector. This is not surprising since only about[17] 0.05% of the ^{32}Cl decays give rise to proton emission, in contrast to about 34% in the case of ^{33}Ar. Some ^{17}Ne peaks, produced from an oxygen contaminant, are visible in Figs. 9 and 10 but are quite weak. The primary peak has been previously identified as due to ^{33}Ar by cross bombardments[33] and by excitation function measurements.[33,73]

The relative intensities of the peaks in Figs. 9 and 10 were compared, taking account of the additional ^{17}Ne strength. All relative

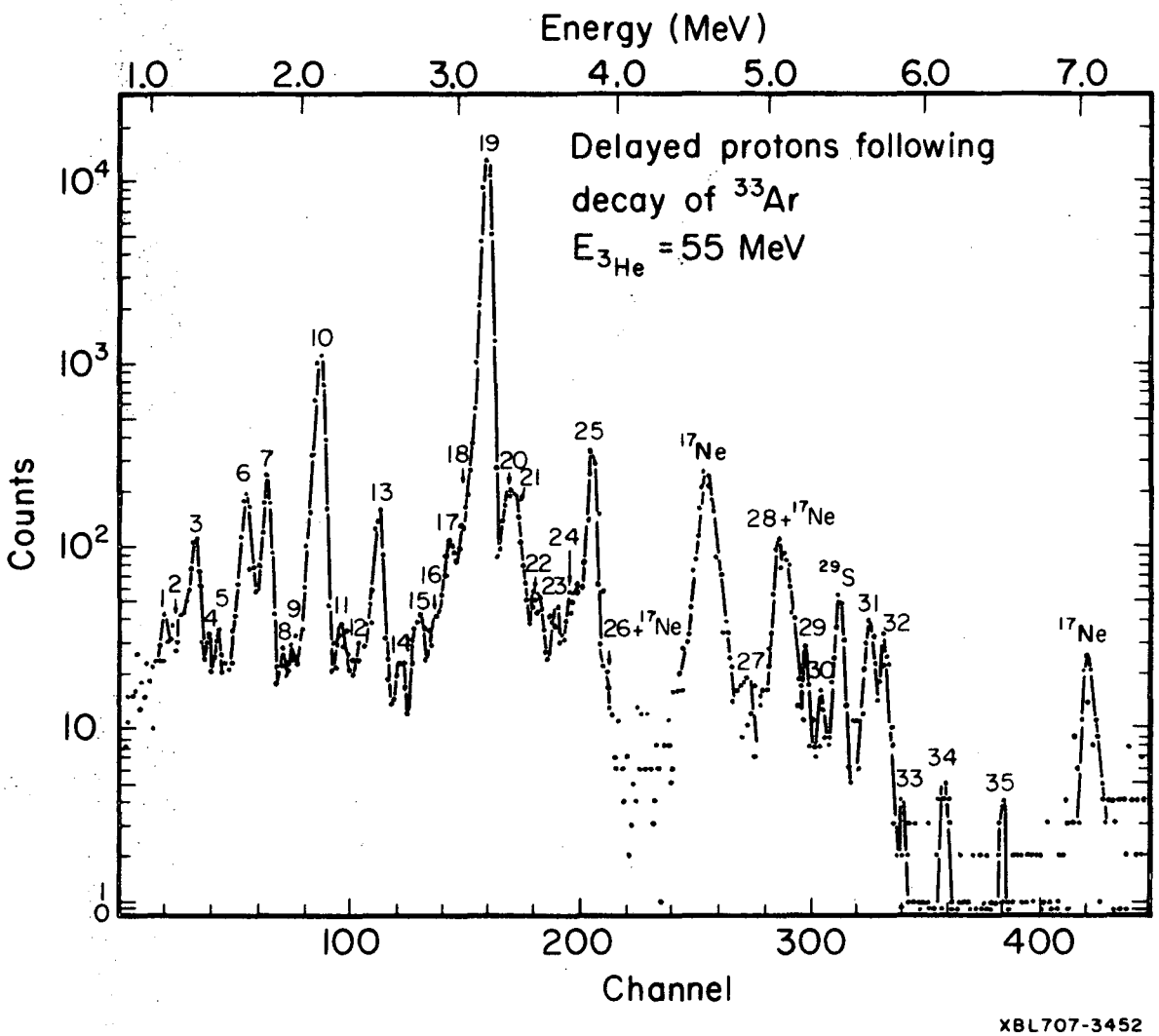

Fig. 9. Spectrum of delayed protons observed in a counter telescope following ^{3}He bombardment of CS_2. All numbered peaks except no. 11 follow the β-decay of ^{33}Ar. Table V gives the energies of numbered peaks.

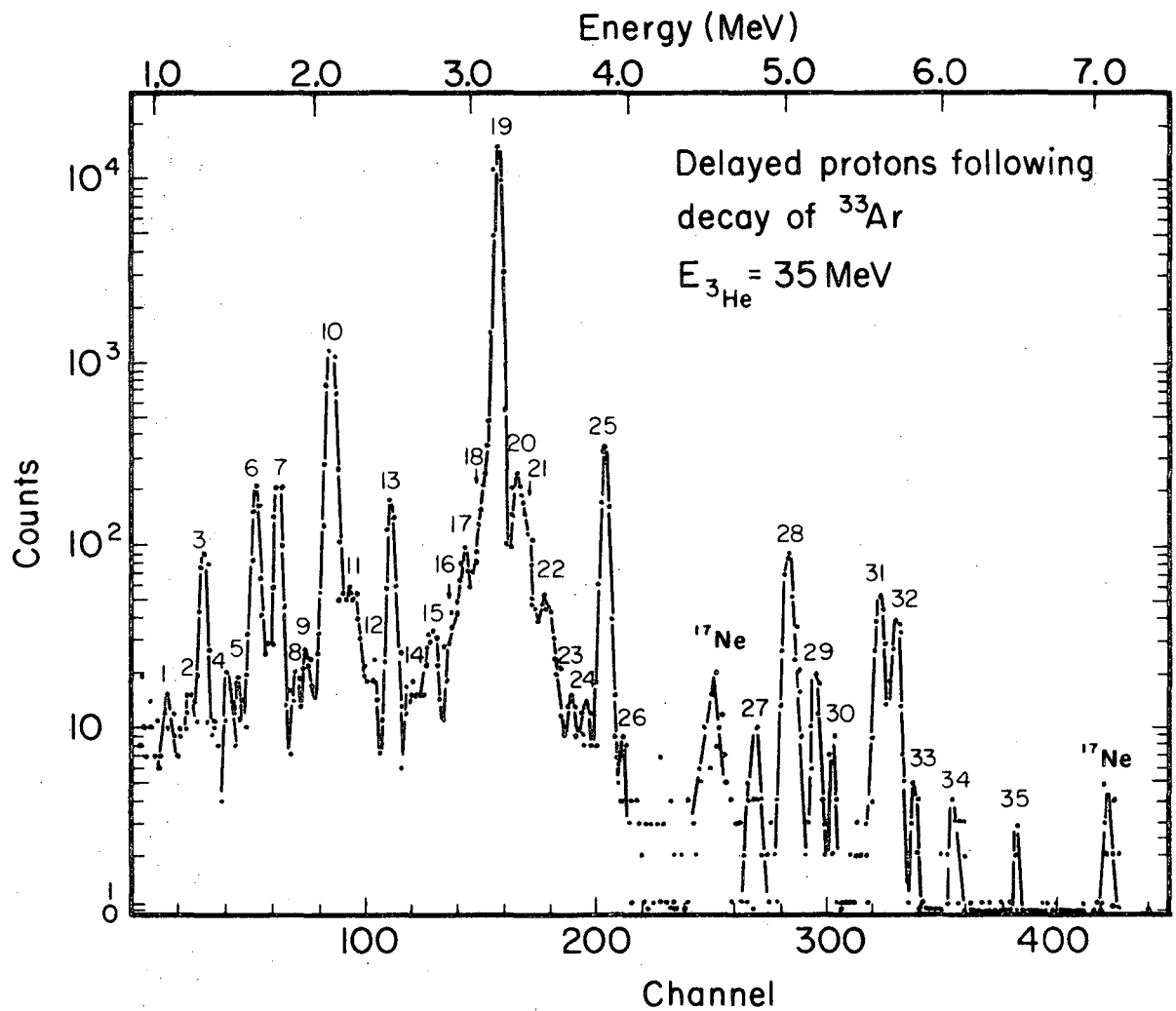

XBL707-3451

Fig. 10. A spectrum of delayed protons taken under conditions identical to those used to obtain that in Fig. 9 except for the lower bombarding energy.

intensities were the same except peak 11 which was much weaker at the higher bombarding energy. Its origin is unknown but it does not seem to follow the decay of ^{33}Ar.

The spectrum in Fig. 9 was used to establish the energies of all the fairly strong peaks. Then they were used to fix the energies of the weaker peaks using the data in Fig. 10. In Fig. 9, peak 19 and the one marked ^{29}S correspond to protons emitted from T = 3/2 analogue states in ^{33}Cl and ^{29}P, respectively. Since these states have been observed in proton resonance work, the laboratory energies of the corresponding proton groups are known to be 3.170 ± 0.004 MeV[74] and 5.437 ± 0.005 MeV.[75] Using these as initial calibration points, the energies of the other peaks were determined. The energies of all the observed proton groups and the deduced level energies in ^{33}Cl are listed in Table V.[59,76,77]

Particle-γ coincidences were recorded to see if any proton peaks could be positively assigned as representing proton emission to the first excited state of ^{32}S (2.24 MeV) rather than to the ground state. No coincidences were observed with 2.24 MeV γ-rays, so all of the stronger peaks (numbers 6, 7, 10, 13, 18-21, and 25) must correspond to decay to the ground state. The good energy resolution and the accurate internal energy calibration make it possible to assign some weak peaks to proton emission to the 2.24-MeV level in ^{32}S by energy balance considerations. Such assignments are shown in Table V. Peak 8 is unassigned because if it goes to the ground state of ^{32}S, a new level at fairly low excitation in ^{33}Cl is required. But if it corresponds to emission to $^{32}S^*$, then the absence of the ground state transition is unexplained. Nevertheless the peak

Table V. Observed proton peaks following ^{33}Ar decay and deduced level energies in ^{33}Cl.

Observed proton energies[a] corresponding to decay to the following ^{32}S states:						Deduced level energies[b] in Cl
	g.s.		2.237 MeV		3.780 MeV	(MeV ± keV)
6	1.692 ± 20					3.973 ± 20
7	1.837 ± 20					4.118 ± 20
10	2.174 ± 20					4.455 ± 20
12	2.439 ± 35		-			4.720 ± 35
13	2.566 ± 15		-			4.847 ± 16
15	2.835 ± 25		-			5.116 ± 25
18	3.165 ± 30		-			5.446 ± 30
19	3.269 ± 4[c]		-			5.550 ± 6[c]
20	3.403 ± 20	1	1.126 ± 35			5.675 ± 17
21	3.469 ± 30	2	1.264 ± 35			5.763 ± 23
22	3.592 ± 35[d]	3	1.364 ± 30			5.882 ± 31
23	3.751 ± 35	4	1.519 ± 35			6.034 ± 25
24	3.859 ± 35	5	1.587 ± 40		-	6.125 ± 26
25	3.973 ± 20		X		-	6.254 ± 20
27	4.984 ± 40	14	2.687 ± 30		X	7.228 ± 25
28	5.189 ± 20	16	2.975 ± 40		X	7.475 ± 18
29	5.342 ± 30	17	3.048 ± 30		X	7.595 ± 22
30	5.486 ± 40		X		X	7.767 ± 40
31	5.803 ± 20	22	3.592 ± 35[d]	9	2.022 ± 30	8.084 ± 17
32	5.902 ± 25	22	3.592 ± 35[d]		X	8.183 ± 25

(continued)

Table V (continued)

Observed proton energies[a] corresponding to decay to the following ^{32}S states:						Deduced level energies[b] in Cl (MeV ± keV)
	g.s.		2.237 MeV		3.780 MeV	
33	6.029 ± 30		X		X	8.310 ± 30
34	6.310 ± 40	26	4.106 ± 35		X	8.609 ± 27
35	6.688 ± 30		X		X	8.969 ± 30

unassigned proton peaks[e]: 8 1.947 ± 30, 11 2.303 ± 35

[a]All observed energies are quoted in the center-of-mass system as (MeV ± keV) and are preceded by under-lined numbers relating them to peaks in the spectra of Figs. 9 and 10. Those spaces marked "X" correspond to proton groups predicted from the deduced energy levels to be within our range of observation, but which were not in fact seen. Those marked "-" represent groups predicted to be outside our range of observation (*i.e.*, $\lesssim$ 1.0 MeV).

[b]The level energies were calculated using 21.005 ± 0.004 MeV as the mass excess of ^{33}Cl; it is a weighted average of the results in Refs. 58, 76, and 77.

[c]The energy of the lowest T = 3/2 state was taken from Ref. 74 and corrected for the ^{33}Cl mass excess.

[d]The weak proton peak at E_{cm} = 3.592 MeV is broad and could involve several groups; it therefore appears more than once in the table.

[e]The possible origin of these peaks is discussed in the text.

follows the decay of ^{33}Ar and was included while calculating relative intensities. The energy levels determined from the proton spectra are compared with previous work in Table VI. The agreement is excellent. Table VII[78] shows the particle branching ratios and reduced-width ratios for all observed states in ^{33}Cl.

Since one allowed β-decay branch was expected to feed an excited state in ^{33}Cl below the proton-separation energy, γ-spectra were taken with a Ge(Li) detector. Figure 11 shows one of the four time-routed spectra. A ^{56}Co source was used to establish the energy scale. With the energy and life-time information, it was possible to identify the origin of most of the peaks in Fig. 11. Table VIII[79] lists the γ-rays, gives their energies, and compares them to previous results.

The 810 keV γ-ray corresponds[58,77] to de-excitation of the first excited state of ^{33}Cl and was identified as following the decay of ^{33}Ar by its half-life. As expected, no other γ-rays that could be associated with the decay of ^{33}Ar were identified in the spectra. The absolute intensity of the 810 keV γ-ray was determined by integrating the γ-ray peak heights. Dead time corrections were determined from a pulser that had been running into the system throughout the experiment. Using the counter efficiencies previously determined and a proton spectrum obtained simultaneously, the γ-ray intensity was found to be 1.42 ± 0.24 times the total delayed-proton intensity.

The γ-ray and delayed-proton measurements combined do not account for all possible β^+-decay branches. The intensity of the allowed transition to the ground state was calculated using the <u>ft</u>-value[58] for the mirror

Table VI. Comparison of observed levels below 6 MeV in ^{33}Cl with previous results.[a]

Present Results (MeV ± keV)	Endt *et al.*[c] (MeV ± keV)	Previous work[b] Gordon[d] (MeV ± keV)	other (MeV ± keV)	$\Gamma^{c,d}$ (MeV)	Average level energy (MeV)	J^{π}
3.973 ± 20	3.984 ± 4	3.982 ± 4		0.0015	3.983 ± 3	$3/2^+$
4.118 ± 20	4.123 ± 4	4.123 ± 4	4.119 ± 10[e]	0.0085	4.123 ± 3	$3/2^+$
4.455 ± 20	4.444	4.441 ± 4		< 0.002	4.442 ± 4	$3/2^+$
4.720 ± 35	4.746	4.751 ± 4		< 0.002	4.751 ± 4	$5/2^-$
4.847 ± 16	4.831	4.837 ± 4		< 0.002	4.838 ± 4	$3/2^+$
5.116 ± 25	5.110 ± 4	5.111 ± 4		0.0015	5.111 ± 4	$3/2^+$
5.446 ± 30	5.455 ± 6			0.032	5.455 ± 6	$1/2^+$
			5.550 ± 6[f]	0.0015[f]	5.550 ± 6	$1/2^+$, T = 3/2
5.675 ± 17	5.656 ± 10[g]			0.100	5.675 ± 17	$(1/2^+, 3/2^+)$
5.673 ± 23	5.743 ± 6			0.040	5.744 ± 6	$1/2^+$
5.882 ± 31	5.884 ± 4[g]			0.001	5.882 ± 31	$(1/2^+, 3/2^+)$

[a]Only those levels below 6 MeV are shown since none above that energy have been reported previously with comparable error bars; our complete results appear in Table V.

[b]All previous results have been corrected, where necessary, to take account of the ^{33}Cl mass excess being 21.005 ± 0.004 MeV.

(continued)

Table VI (continued)

[c]See Ref. 58.

[d]$^{32}S(p,\gamma)^{33}Cl$; see Ref. 77.

[e]$^{32}S(^{3}He,d)^{33}Cl$; see Ref. 76.

[f]$^{32}S(p,p)^{32}S$; see Ref. 74.

[g]The spins and parities assigned these states in Ref. 58 are not consistent with their being fed by allowed β^{+}-decay from ^{33}Ar. Nevertheless, the agreement in energies and in observed decay channels makes it appear plausible that we are seeing the same states. Since the possibility of unresolved doublets cannot be ruled out, the two energies were not averaged.

Table VII. Particle branching ratios from states in ^{33}Cl.

^{33}Cl (MeV)	Observed relative branching ratios [$^{32}S(2.24)/^{32}S(0.00)$]	$\gamma^2(2.24)^a/\gamma^2(0.00)$ 1/2+	$\gamma^2(2.24)^a/\gamma^2(0.00)$ 3/2+	Observed relative branching ratios [$^{32}S(3.78)/^{32}S(0.00)$]	$\gamma^2(3.78)^a/\gamma^2(0.00)$ 1/2+	$\gamma^2(3.78)^a/\gamma^2(0.00)$ 3/2+
5.675	0.027 ± 0.011	84	0.41			
5.744	0.052 ± 0.017	83	0.50			
5.882	> 0.87	> 960	> 6.9			
6.034	2.7 ± 1.7	1400	12.4			
6.125	2.8 ± 2.7	1180	11.8			
6.254	< 0.028	< 8.3	< 0.09			
7.228	2.1 ± 0.8	67	2.5			
7.475	0.26 ± 0.04	5.9	0.27			
7.595	5.7 ± 0.8	121	5.6			
7.767	b	-	-			
8.084	< 1.6	< 19	< 1.4	0.36 ± 0.06	4.1	28
8.183	< 2.5	< 36	< 2.2			
8.310	< 0.15	< 1.3	< 0.13			
8.609	0.48 ± 0.28	3.6	0.36			
8.969	< 2.0	< 13	< 1.5			

[a] γ^2 is the reduced width. This ratio is obtained from the observed value by dividing each branching ratio by its respective penetration factor,[78] assuming either $1/2^+$ or $3/2^+$ as the J^π for the state in ^{33}Cl. The interaction radius was taken to be 5.2 fm.

[b] No limit could be set on the intensity of this branch since it coincided with another proton group.

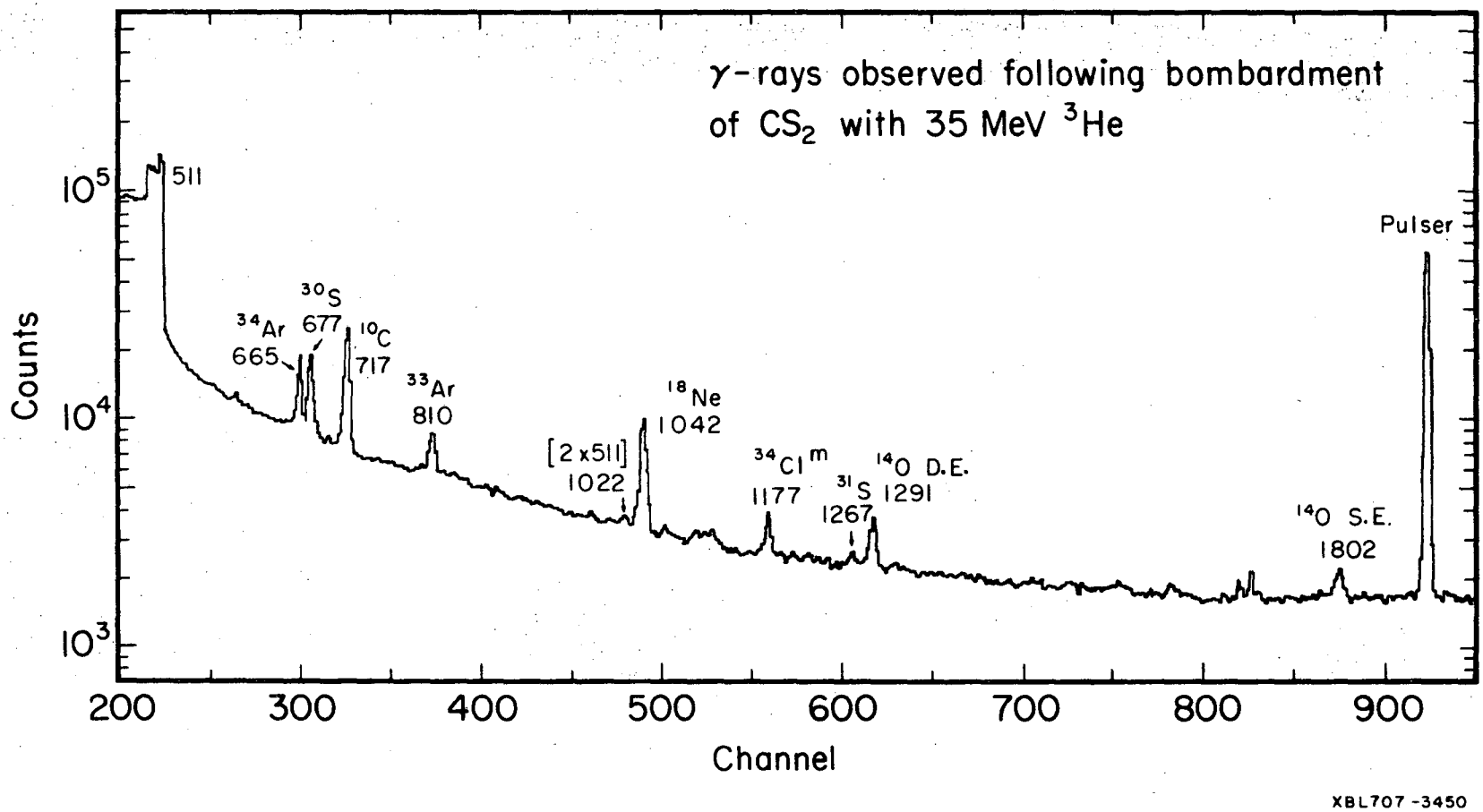

Fig. 11. A γ-ray spectrum taken with a Ge(Li) detector following ^{3}He bombardment of CS_2. The 511-keV γ-ray has folded over upon itself several times.

Table VIII. γ-rays observed following bombardment of CS_2 with 35-MeV ^3He.

Observed γ-rays (keV)	Transition responsible	Previously measured: γ Energy (keV)	β^+ half-life (sec)
665 ± 2	$^{34}Ar(\beta^+)^{34}Cl^{***}(\gamma)^{34}Cl$	664.6 ± 0.3[a]	b
677 ± 2	$^{30}S(\beta^+)^{30}P^{*}(\gamma)^{30}P$	677.8 ± 0.9[c]	1.4[c]
717.3 ± 0.8[d]	$^{10}C(\beta^+)^{10}B^{*}(\gamma)^{10}B$	717.3 ± 0.8[e]	19.4[e]
810 ± 2	$^{33}Ar(\beta^+)^{33}Cl^{*}(\gamma)^{33}Cl$	810 ± 3[f]	0.173[g]
1042 ± 2	$^{18}Ne(\beta^+)^{18}F^{**}(\gamma)^{18}F$	1041.7 ± 0.6[h]	1.67[i]
1177 ± 2	$^{34}Cl^{m}(\beta^+)^{34}S^{**}(\gamma)^{34}S^{*}$	1177.0 ± 1.2[c]	1.57[c]
1267 ± 3	$^{31}S(\beta^+)^{31}P^{*}(\gamma)^{31}P$	1266.1 ± 0.2[c]	2.61[c]
1290.79 ± 0.06[d]	$^{14}O(\beta^+)^{14}N^{*}(\gamma D.E.)^{14}N$	1290.79 ± 0.06[j]	71.0[j]
1801.80 ± 0.06[d]	$^{14}O(\beta^+)^{14}N^{*}(\gamma S.E.)^{14}N$	1801.80 ± 0.06[j]	71.0[j]

[a] H. D. Graber and G. J. Harris, Phys. Rev. 188, 1685 (1969).

[b] Values quoted in Ref. 58 are 1.2 ± 0.3 sec and 0.85 ± 0.10 sec. Our results indicate a half-life of 0.91 ± 0.05 sec.

[c] See Ref. 58.

[d] Used as calibration.

[e] See Ref. 6.

[f] Average of results quoted in Refs. 58 and 77.

[g] Obtained from the present delayed-proton results.

[h] E. K. Warburton, J. W. Olness, and A. R. Poletti, Phys. Rev. 155, 1164 (1967).

[i] See Ref. 51.

[j] See Ref. 79.

decay, $^{33}P \xrightarrow{\beta^-} {}^{33}S$, and increasing it by 6% to take account of the trend of known deviations from mirror symmetry. (See Sec. II C.) Then the relative intensities and ft-values for all significant β-branches from ^{33}Ar could be calculated. These results are listed in Table IX. The corresponding decay scheme is shown in Fig. 12.

Since the spin of ^{33}Ar is expected to be $1/2^+$, like its mirror ^{33}P, all states fed by β-branches whose log ft is $\leqslant 6.0$ probably have $J^\pi = (1/2,3/2)^+$. The β-transition to the 4.751-MeV state has a log ft of 6.39 and has previously been assigned J = 5/2. This ft-value is in the first-forbidden range, but not in the second-forbidden range. Thus the state probably has negative parity. Table VI contains the spin and parity assignments of states below 6 MeV in ^{33}Cl. Unique assignments result from previous work.

Shell model calculations of the levels in ^{33}Cl have been made.[80] They predict sixteen $1/2^+$ or $3/2^+$ levels below 9 MeV, whereas the experiment indicates twenty-two allowed transitions. The discrepancy is doubtless due to the limited space considered in the calculation; only $2s_{1/2}$ and $1d_{3/2}$ shells were allowed. Since other orbitals are probably required, quantitative comparison of theory and experiment is not justifiable.

B. ^{17}Ne Decay

The study of ^{17}Ne required a combination of delayed-proton and p-γ coincidence measurements. The latter measurements assisted in determining the proper decay scheme. As in the previous section, the delayed-proton data allowed the determination of level energies and ft-values.

Table IX. β^+ branching ratios and ft values for $^{33}Ar \xrightarrow{\beta^+} {}^{33}Cl$.

Energy level[a] in ^{33}Cl (MeV)	Proportion of proton emissions (%)	Branching ratio from ^{33}Ar (%)	ft[b] (sec)	log ft (sec)
0.000	-	18.1 ± 1.9[c]	$(1.06 \pm 0.11)\times10^5$	5.03 ± 0.05
0.810	-	48.1 ± 3.6	$(2.74 \pm 0.21)\times10^4$	4.44 ± 0.03
3.983	1.19 ± 0.05	0.40 ± 0.04	$(5.14 \pm 0.55)\times10^5$	5.71 ± 0.05
4.123	1.26 ± 0.05	0.43 ± 0.05	$(4.32 \pm 0.53)\times10^5$	5.64 ± 0.05
4.442	7.41 ± 0.13	2.50 ± 0.26	$(5.75 \pm 0.64)\times10^4$	4.76 ± 0.05
4.751	0.14 ± 0.02	0.047 ± 0.008	$(2.45 \pm 0.43)\times10^6$	6.39 ± 0.08
4.838	0.92 ± 0.05	0.31 ± 0.04	$(3.46 \pm 0.43)\times10^5$	5.54 ± 0.05
5.111	0.24 ± 0.03	0.081 ± 0.013	$(1.06 \pm 0.17)\times10^6$	6.03 ± 0.07
5.455	1.68 ± 0.06	0.57 ± 0.06	$(1.11 \pm 0.13)\times10^5$	5.05 ± 0.05
5.550	78.9 ± 0.8	26.7 ± 2.7	$(2.18 \pm 0.24)\times10^3$	3.34 ± 0.05
5.675	1.63 ± 0.06	0.55 ± 0.06	$(9.4 \pm 1.1)\times10^4$	4.97 ± 0.05
5.744	1.09 ± 0.04	0.37 ± 0.04	$(1.31 \pm 0.16)\times10^5$	5.12 ± 0.05
5.882	$0.68^{+0.38}_{-0.19}$	$0.23^{+0.13}_{-0.07}$	$(1.84^{+0.57}_{-1.04})\ 10^5$	5.26 ± 0.18
6.034	0.08 ± 0.02	0.027 ± 0.007	$(1.35 \pm 0.36)\times10^6$	6.13 ± 0.12

(continued)

Table IX (continued)

Energy level[a] in ^{33}Cl (MeV)	Proportion of proton emissions (%)	Branching ratio from ^{33}Ar (%)	ft[b] (sec)	log ft (sec)
6.125	0.05 ± 0.02	0.017 ± 0.007	$(1.96 \pm 0.92)\times10^{6}$	6.29 ± 0.22
6.254	1.73 ± 0.06	0.58 ± 0.06	$(5.01 \pm 0.60)\times10^{4}$	4.70 ± 0.05
7.228	0.12 ± 0.02	0.041 ± 0.008	$(2.23 \pm 0.47)\times10^{5}$	5.35 ± 0.09
7.475	0.86 ± 0.04	0.29 ± 0.03	$(2.24 \pm 0.29)\times10^{4}$	4.35 ± 0.06
7.595	0.74 ± 0.04	0.25 ± 0.03	$(2.17 \pm 0.31)\times10^{4}$	4.34 ± 0.06
7.767	0.03 ± 0.01	0.010 ± 0.003	$(4.2 \pm 1.3)\times10^{5}$	5.62 ± 0.14
8.084	$0.67^{+0.38}_{-0.19}$	$0.23^{+0.13}_{-0.07}$	$(1.07^{+0.37}_{-0.67})\times10^{4}$	4.05 ± 0.20
8.183	$0.41^{+0.38}_{-0.19}$	$0.14^{+0.13}_{-0.07}$	$(1.47^{+0.75}_{-1.37})\times10^{4}$	4.17 ± 0.30
8.310	0.05 ± 0.01	0.017 ± 0.004	$(9.5 \pm 2.2)\times10^{4}$	4.98 ± 0.10
8.609	0.05 ± 0.01	0.017 ± 0.004	$(5.2 \pm 1.4)\times10^{4}$	4.71 ± 0.12
8.969	0.01 ± 0.005	0.003 ± 0.0015	$(1.22 \pm 0.64)\times10^{5}$	5.09 ± 0.25
$[E_p = 1.947]$[d]	0.07 ± 0.02	0.024 ± 0.007		

(continued)

Table IX (continued)

[a]The values below 6 MeV are averages taken from Table VI. Above that energy they are from the present work only.

[b]The ft values are calculated using (-9.400 ± 0.050)MeV as the mass excess of ^{33}Ar and (173.0 ± 2.0)ms as its half-life. The mass was calculated using the isobaric mass formula and the results in Refs. 5 and 74.

[c]This ratio is calculated by comparison with the mirror ^{33}P decay.

[d]The center-of-mass energy of this proton group is listed since the level from which it originates is uncertain.

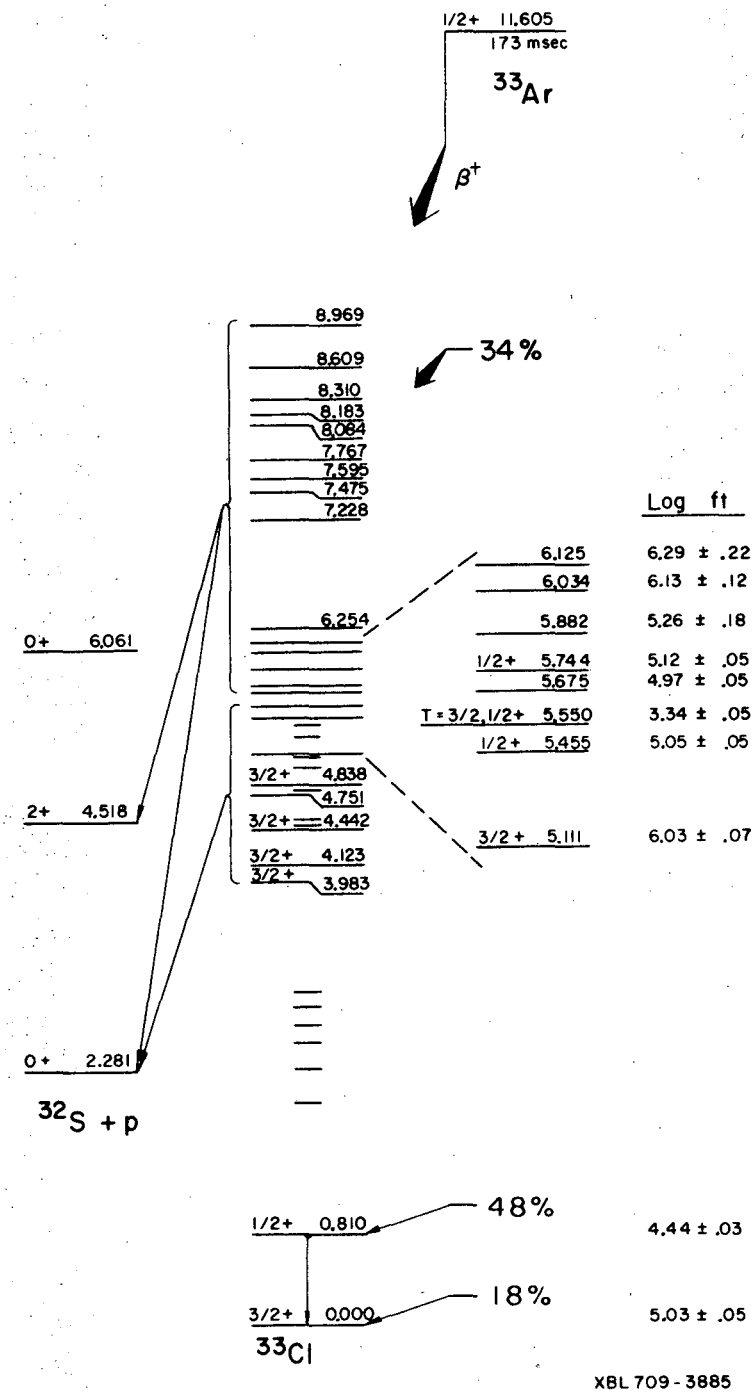

Fig. 12. Proposed decay scheme of ^{33}Ar. The decay of the 8.084-MeV state to the second excited state of ^{32}S has not been indicated for the sake of clarity. The ^{33}Cl level energies are taken from Table VI for those levels below 6 MeV and from the present work for levels above 6 MeV.

The large energy range (1 to 11 MeV) spanned by the ^{17}Ne proton groups made it necessary to investigate the upper and lower portions of the delayed-proton spectrum separately.

Figures 13 and 14 show delayed-proton spectra following 45-MeV ^{3}He bombardment of TiO_2 using different counter telescopes. The spectrum in Fig. 13 was acquired using a 50 μm ΔE detector while that in Fig. 14 was obtained with a 14 μm detector. The former spectrum only extends down to 2.5 MeV because less energetic protons could not penetrate the 50 μm ΔE detector. On the other hand, the peak intensities above 8 MeV in the latter spectrum are unreliable because the higher energy protons lose very little energy in the 14 μm ΔE counter.

At this bombarding energy, the only two known delayed-proton emitters that can be produced from titanium or oxygen are ^{13}O and ^{17}Ne. As was argued in the previous section, ^{13}O does not contribute to the spectra, so ^{17}Ne must be the source of the proton groups. Additionally the main peaks in the spectra have been identified as following the decay of ^{17}Ne by cross bombardments and excitation functions.[26,27]

Because peak 10, the most intense ^{17}Ne proton group, appeared in the ^{33}Ar spectra shown in Figs. 9 and 10, its energy was known. (See Sec. IV A.) Peak 17 corresponds to decay of the lowest T = 3/2 analogue state in ^{17}F. Since the excitation energy of this state is well known,[5] peak 17 provides a second energy calibration point. Additionally, when oxygen gas was bombarded in a target chamber that had been left uncleaned after a bombardment of CS_2, a ^{17}Ne spectrum contaminated with ^{33}Ar was obtained. Since the main ^{33}Ar group arises from the decay of a known[74]

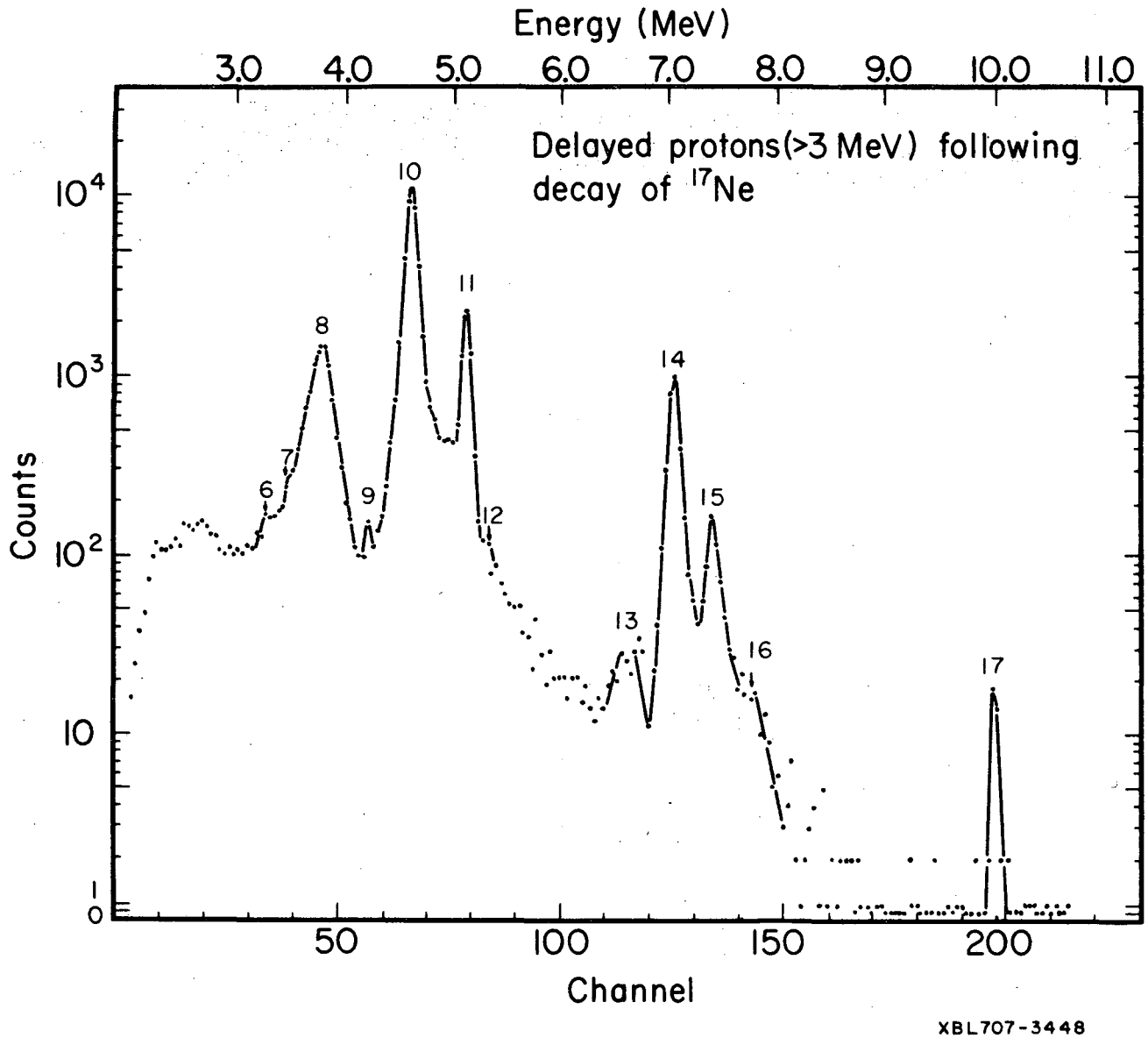

Fig. 13. Spectrum of delayed protons observed in a counter telescope containing a 50 μm ΔE counter following 35-MeV ^{3}He bombardment of oxidized titanium foils. The energies of all numbered peaks are given in Table X.

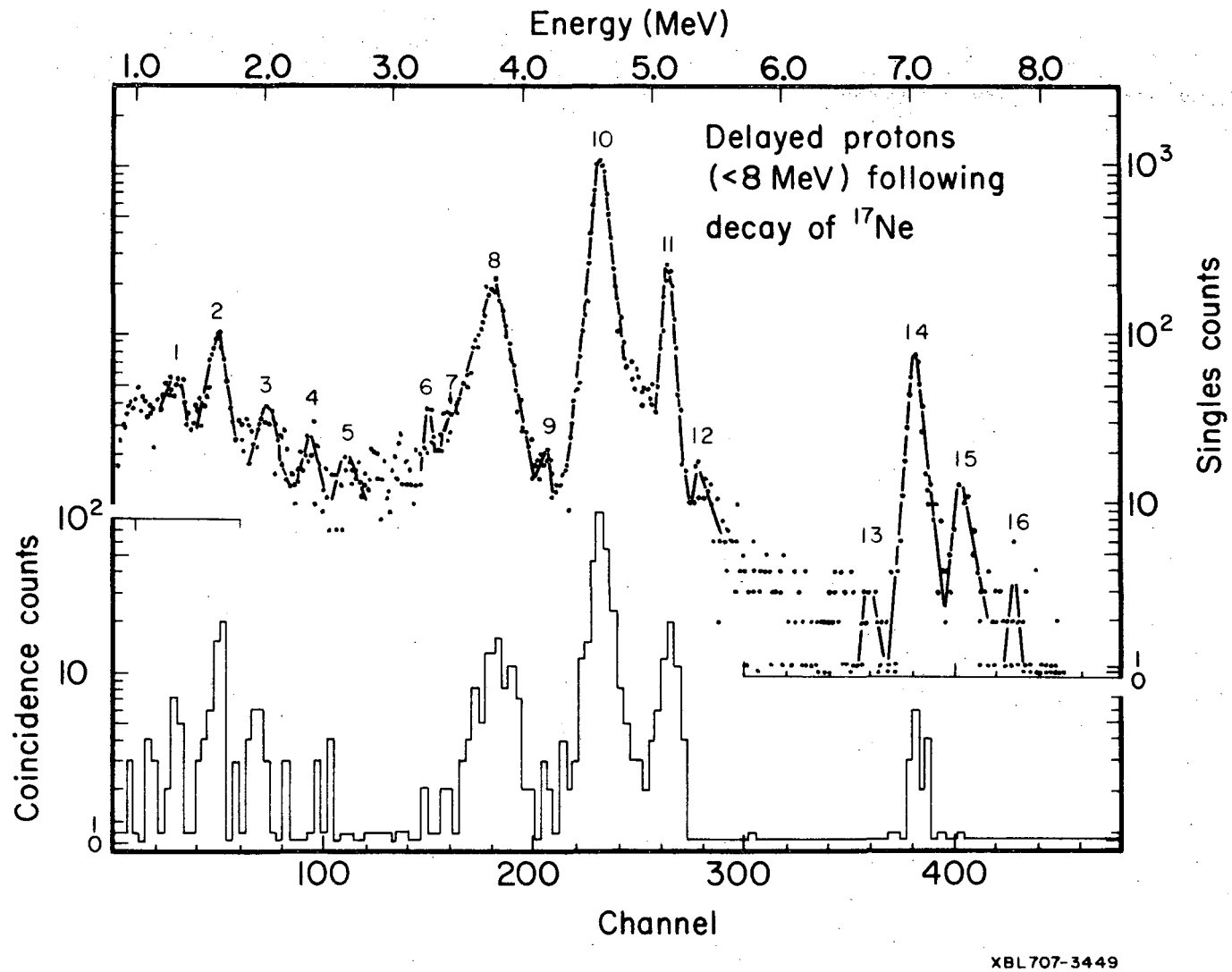

Fig. 14. The upper portion of the figure is a proton spectrum taken under similar conditions to those of Fig. 13 except a 14 μm ΔE counter was used. The lower spectrum shows those protons which were in coincidence with a 511-keV γ-ray and was taken simultaneously with the upper spectrum.

T = 3/2 analogue state, it provides an excellent calibration point. Table X contains the energies of all the observed proton peaks.

In the case of ^{17}Ne decay, proton groups can result from proton emission to several states in ^{16}O. The measured energies of the groups are usually sufficient to solve this problem, but the first two excited states of ^{16}O are separated by only 80 keV, creating some difficulty. Fortunately the first excited state of ^{16}O has a special property; it decays by internal pair conversion because 0^+ to 0^+ γ-transitions are forbidden. Thus proton decays to the first excited state of ^{16}O are accompanied by two positrons, one from internal pair conversion and one from the preceding β^+-decay. All other proton groups are associated with a single positron. Thus, a proton group which decays via the ^{16}O first excited state should be associated with twice as much 511-keV annihilation radiation as the other proton groups.

The histogram at the base of Fig. 14, obtained simultaneously with the spectrum above it, contains those protons that were in coincidence with annihilation radiation. The percentage of coincidence protons for peaks 1, 2, 3, and 10 are compared in Table XI. The results indicate that the former three peaks probably correspond to proton decays to the first excited state of ^{16}O. The measured energies for these groups are also consistent with this assignment.

The final ^{17}F energy levels derived from analysis of the proton groups are listed in Table XII,[81-85] and the accompanying decay scheme is shown in Fig. 15. The present results resolve the discrepancy between Salisbury _et al._[81] and Harris _et al._[82] in favor of the latter. While momentum broadening makes it difficult to extract level widths from

Table X. Observed proton peaks following ^{17}Ne decay and deduced energies in ^{17}F.

Observed proton energies,[a] corresponding to decay to the following ^{16}O states:										Deduced level energies in ^{17}F (MeV ± keV)
	g.s.		6.052 MeV		6.131 MeV		6.916 MeV		7.115 MeV	
4	2.484 ± 30									3.084 ± 30
8	4.009 ± 15									4.609 ± 15
10	4.880 ± 10									5.480 ± 10
11	5.437 ± 10									6.037 ± 10
12	5.806 ± 30									6.406 ± 30
13	7.108 ± 30		X		-		-			7.708 ± 30
14	7.474 ± 10	1	1.434 ± 25		X		-		-	8.075 ± 10
15	7.837 ± 10	2	1.771 ± 30		X		-		-	8.436 ± 10
16	8.232 ± 30	3	2.163 ± 35		X		X		X	8.825 ± 25
17	10.597 ± 4[b]		X	9	4.458 ± 10	7	3.658 ± 30	6	3.481 ± 20	11.197 ± 4[b]
	unassigned proton peak[c]:			5	2.825 ± 30					

[a]All observed energies are quoted in the center-of-mass system as (MeV ± keV) and are preceded by underlined numbers relating them to peaks in the spectra of Figs. 13 and 14. Those spaces marked "X" correspond to proton groups predicted from the deduced energy levels to be within our range of observation, but which

(continued)

Table X (continued)

were not in fact seen. Those marked "-" represent groups predicted to be outside our range of observation ($\lesssim$ 1 MeV).

[b]The energy of this level was taken from Ref. 5 and the proton peak corresponding to its ground-state decay was used in part to establish the calibration.

[c]The possible origin of this peak is discussed in the text.

Table XI. Results of proton-γ (511 keV) coincidence measurements for ^{17}Ne decay.

	Proton energy (MeV)	Proton-singles counts	Proton-γ(511 keV) coincidence counts[a]	coincidences / singles (%)
1	1.434	289 ± 20	12.1 ± 5.3	4.2 ± 1.9
2	1.771	638 ± 28	39.7 ± 7.1	6.2 ± 1.1
3	2.163	177 ± 15	7.3 ± 3.3	4.1 ± 1.9
10	4.880	8889 ± 95	266.4 ± 16.8	2.5 ± 0.2

[a]These numbers have been corrected for the change- and background-coincidence counting rate.

Table XII. Comparison of observed energy levels in ^{17}F with previous results.

Present Results (MeV ± keV)	Previous work: Salisbury *et al.*[a] (MeV ± keV)[d]	Harris *et al.*[b] (MeV ± keV)[d]	Dangle *et al.*[c] (MeV ± keV)[d]	other (MeV ± keV)	$\Gamma^{a,c}$ (MeV)	J^{π}
3.084 ± 30		3.10 ± 20		3.106 ± 7[e]	0.020	$1/2^-$
4.609 ± 15	4.698 ± 10	4.60 ± 20			0.240	$3/2^-$
5.480 ± 10	5.526 ± 10	5.47 ± 20			0.073	$3/2^-$
6.037 ± 10	6.046 ± 10				0.030	$1/2^-$
6.406 ± 30				6.43 ± 80[f]		$(1/2,3/2)^-$
7.708 ± 30			7.75 ± 10[g]		0.190	$(1/2,3/2)^-$
8.075 ± 10			8.09 ± 10[g]		0.110	$(1/2,3/2)^-$
8.436 ± 10			8.45 ± 10[g]		0.045	$(1/2,3/2)^-$
8.825 ± 25						$(1/2,3/2)^-$
				11.197 ± 4[h]	0.0005[i]	$1/2^-$,T=3/2

[a] $^{16}O(p,p)^{16}O$; see Ref. 81.

[b] $^{16}O(p,p)^{16}O$; see Ref. 82.

[c] $^{16}O(p,p)^{16}O$, $^{16}O(p,p')^{16}O$, $^{16}O(p,\alpha)^{13}N$; see Ref. 83.

[d] The uncertainty quoted with these results includes only the uncertainty in the incident proton energy. The discrepancy between references 81 and 82 indicates that the errors in determining some resonance energies are

(continued)

Table XII (continued)

considerably larger.

[e] $^{16}O(p,p)^{16}O$; see Ref. 84.

[f] Delayed proton emission; see Ref. 27.

[g] The spins and parities assigned these states in Ref. 83 are not consistent with their being fed by allowed β^+-decay from ^{17}Ne. Nevertheless, the agreement in energies and in observed decay channels makes it appear plausible that we are observing the same state. The possibility of unresolved doublets cannot, of course, be ruled out.

[h] See Ref. 5.

[i] See Ref. 85.

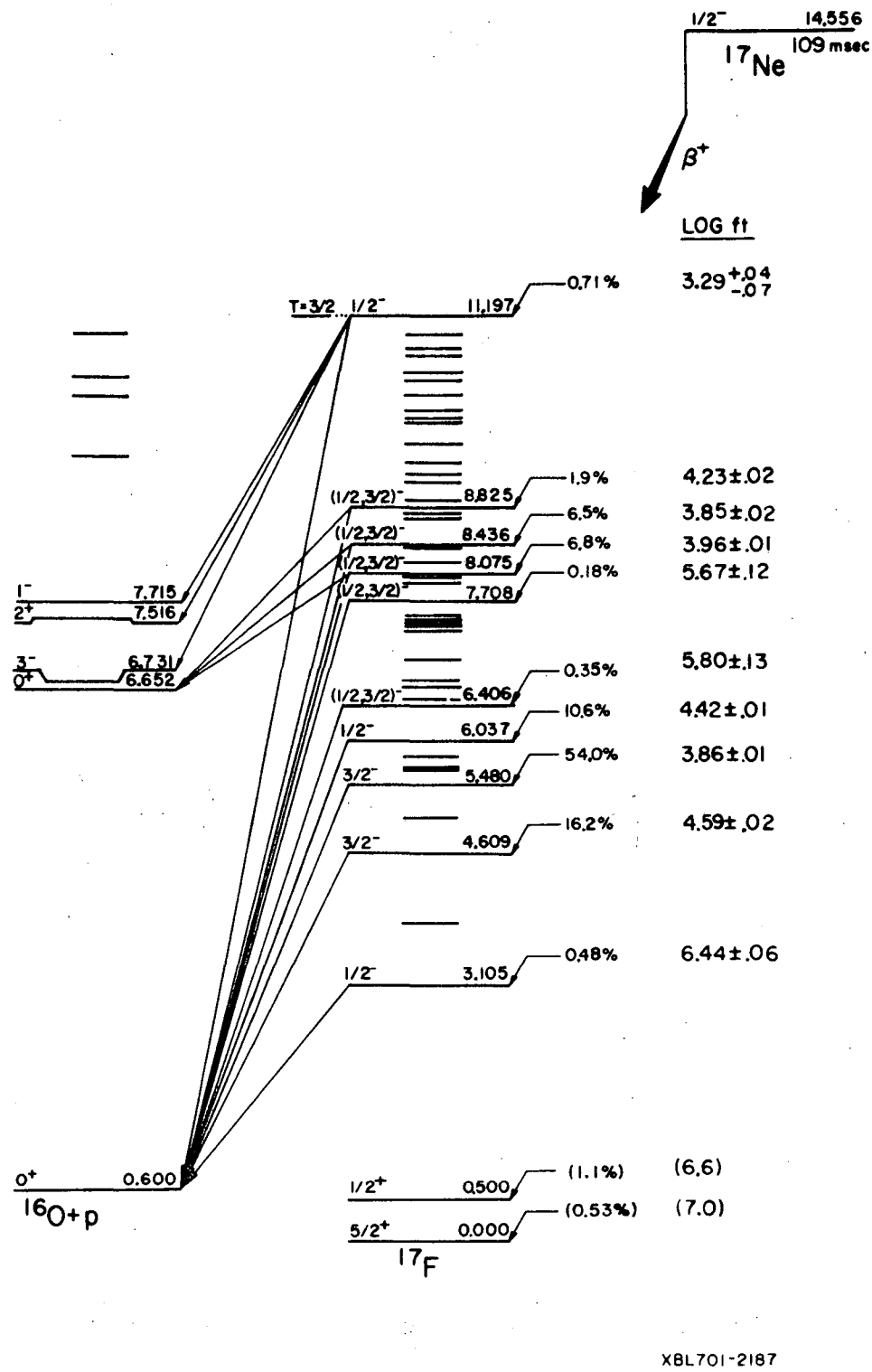

Fig. 15. Proposed decay scheme of ^{17}Ne. Except for the T = 3/2 state, the ^{17}F level energies above 4 MeV result from the present work.

observed proton peak widths, the widths of the peaks in Figs. 13 and 14 are in rough agreement with the level widths listed in Table XII.

This agreement is useful since peaks 6 and 9 are quite narrow, and can be assigned to result from decay of the T = 3/2 state based on their widths as well as on their energies. The T = 3/2 state in ^{17}F is at 11.197 MeV and therefore has many available decay channels, all listed in Table XIII.[86] The table also contains calculated penetration factors for each branch and intensities and branching ratios for all observed branches. The limits on the α-particle branches were set from spectra of all events stopping in the ΔE counter. In the case of the predicted 5.379-MeV α-group, the limit was obtained by searching for identified α-particles using the 14 μm ΔE counter. Of those unobserved decays for which no upper limit could be set, only that to the 1^- state at 9.614 MeV is predicted to be significant. Table XIV contains similar branching and reduced-width ratios for the T = 1/2 states.

Table XV contains the relative β-transition intensities to all observed proton-emitting states in ^{17}F. The errors on the value for the 11.197-MeV state include the effect of the limits listed in Table XIV as well as a limit of < 0.05 for the unobserved decay branch to the 9.614-MeV state. This limit is based on the calculated penetration factor and the observed intensity of proton emission to the 1^- state at 7.115 MeV.

Values of $\underline{f_1 t}$ from the decay of the mirror nucleus, ^{17}N, were used to predict the strength of the first-forbidden decays to the ground and first-excited states of ^{17}F. (See Sec. II B.) Then $\underline{ft}$-values were calculated for all observed levels. The results are compiled in Table XV. The

Table XIII. Energetically-allowed particle decays of the 11.197-MeV, T = 3/2 state in ^{17}F.

	Final state[a] (MeV)	J^{π}	Energy of decay particle[b] (MeV)	Penetration Factor, P[c]	Observed intensity, I[d] (%)	I/P[e]	Particle branching ratio[f] %
$p + {}^{16}O$	0.000	0^+	10.597	2.3	0.074 ± 0.016	0.032	10 ± 2[g]
	6.052	0^+	4.545	1.0	< 0.02	< 0.02	
	6.131	3^-	4.466	0.4	0.160 ± 0.015	0.40	22 ± 2[g]
	6.916	2^+	3.681	0.8	0.174 ± 0.040	0.22	24 ± 6
	7.115	1^-	3.482	1.1	0.313 ± 0.025	0.28	44 ± 4
	8.870	2^-	1.727	0.02	h		
	9.614	1^-	0.983	0.10	-		
	9.847	2^+	0.750	0.009	-		
	10.353	4^+	0.244	$< 10^{-8}$	-		
$a + {}^{13}N$	0.00	$1/2^-$	5.379	2.3	< 0.05	< 0.022	
	2.366	$1/2^+$	3.013	0.4	< 0.05	< 0.125	
	3.509	$3/2^-$	1.870	0.008	-		
	3.547	$5/2^+$	1.832	0.001	-		

[a]The energy levels of ^{16}O are taken from Browne and Michael,[86] those in ^{13}N come from the review of

(continued)

Table XIII (continued)

Ajzenberg-Selove.[79]

[b]These energies are expressed in the center-of-mass system.

[c]$P = kR/(F_L^2 + G_L^2)$ evaluated at a radius of $1.25(A_1^{1/3} + A_2^{1/3})$ fm, where F_L and G_L are the regular and irregular Coulomb functions, respectively, taken from Ref. 78, and L is the lowest allowed angular-momentum transfer.

[d]These intensities are expressed as percentages of the total proton-decay of ^{17}Ne. Spaces marked "-" correspond to predicted energies outside the range of observation.

[e]I/P is the % intensity (column 6) divided by the penetration factor (column 5).

[f]This branching refers only to the particle decay of the 11.197-MeV state in ^{17}F.

[g]These numbers agree well with results from the $^{15}N(^3He,n)^{17}F(11.20)(p)^{16}O$ reaction [A. B. MacDonald, E. G. Adelberger, H. B. Mak, D. Ashery, A. P. Shukla, C. L. Cocke, and C. N. Davids, Phys. Letters 31B, 119 (1970)] where the branching ratio to the ^{16}O ground state is determined to be 9 ± 2% and to the unresolved 6.05-MeV and 6.13-MeV states, 23 ± 5%.

[h]No limit could be set on the intensity of this branch since it coincided with another proton group.

Table XIV. Particle branching ratios from T = 1/2 states in ^{17}F.

^{17}F State (MeV)	Observed relative branching ratio [$^{16}O(6.05)/^{16}O(0.00)$]	$\gamma^2(6.05)/\gamma^2(0.00)^a$
7.708	< 5.0	< 240
8.075	0.49 ± 0.02	7.9
8.436	6.0 ± 0.5	57
8.825	8.2 ± 1.2	52

[a] γ^2 is the reduced width. This ratio is obtained from column 2 by dividing the branching ratios by their respective penetration factors.

Table XV. β^+ branching ratios and ft values for $^{17}Ne \xrightarrow{\beta^+} {}^{17}F$.

Energy level in ^{17}F (MeV)	Proportion of proton emissions (%)	Branching ratio from ^{17}Ne (%)	ft[a] (sec)	log ft (sec)
0.000	-	0.53 ± 0.16[b]	$(8.85 \pm 2.70)\times10^6$	6.95 ± 0.13
0.500	-	1.1 ± 0.5[b]	$(3.56 \pm 1.60)\times10^6$	6.55 ± 0.21
3.105[c]	0.49 ± 0.07	0.48 ± 0.07	$(2.78 \pm 0.41)\times10^6$	6.44 ± 0.06
4.609	16.5 ± 0.7	16.2 ± 0.7	$(3.91 \pm 0.18)\times10^4$	4.59 ± 0.02
5.480	54.9 ± 0.5	54.0 ± 0.7	$(7.19 \pm 0.16)\times10^3$	3.86 ± 0.01
6.037	10.8 ± 0.2	10.6 ± 0.2	$(2.61 \pm 0.07)\times10^4$	4.42 ± 0.01
6.406	0.36 ± 0.10	0.35 ± 0.10	$(6.24 \pm 1.82)\times10^5$	5.80 ± 0.13
7.708	0.18 ± 0.05	0.18 ± 0.05	$(4.70 \pm 1.30)\times10^5$	5.67 ± 0.12
8.075	6.94 ± 0.1	6.83 ± 0.11	$(9.19 \pm 0.29)\times10^3$	3.96 ± 0.01
8.436	6.61 ± 0.26	6.51 ± 0.26	$(7.02 \pm 0.34)\times10^3$	3.85 ± 0.02
8.825	1.93 ± 0.06	1.90 ± 0.06	$(1.68 \pm 0.08)\times10^4$	4.23 ± 0.02
11.197	$0.72^{+0.10}_{-0.05}$	$0.71^{+0.10}_{-0.05}$	$(1.93^{+0.17}_{-0.29})\times10^3$	$3.29^{+0.04}_{-0.07}$
$[E_p = 2.825]$[d]	0.55 ± 0.05	0.54 ± 0.05		

(continued)

Table XV (continued)

[a]The *ft* values are calculated using (16.058 ± 0.026) MeV as the mass excess[49] of ^{17}Ne and (109.0 ± 1.0) ms as its half-life.

[b]These ratios are calculated by comparison with the mirror ^{17}N decay.

[c]This energy is the average of our present result with those listed in Table XII.

[d]The center-of-mass energy of this proton group is listed since the level from which it originates is uncertain.

mass of ^{17}Ne used was calculated[49] from the isobaric multiplet mass formula, since comparably accurate experimental measurements do not yet exist.

A log ft of < 6.0 generally indicates an allowed transition, which in this case requires $J^{\pi} = (1/2, 3/2)^{-}$ for all ^{17}F states observed above 4 MeV. When unique spin and parity values are indicated in Fig. 15, they result from earlier work. One proton group associated with the decay of ^{17}Ne (that at 2.825 MeV) was not assigned to any level in ^{17}F but was used in determining the proton intensities of Table XV. If this group were assumed to feed the ground state of ^{16}O, a new level at low excitation in ^{17}F must be proposed. On the other hand, the absence of the ground state transition must be explained if decay to an excited state is assumed.

Calculations of ^{17}F levels which allowed up to two particles in the (2s,1d)-shell and one hole in the 1p-shell have been performed.[87] Ten $1/2^{-}$ or $3/2^{-}$ levels are predicted below 10 MeV and nine such levels were observed. Since levels above 8 MeV to which the β-decay log ft-values were > 5.5 could not have been observed, the agreement is excellent. The success of these calculations[37,87] in predicting the weak allowed decay to the 3.105-MeV state will be treated later in the discussion of anti-analogue states.

C. ^{13}O Decay

In contrast to the two previous cases, ^{13}O was produced by a proton-induced reaction, ^{14}N(p,2n)^{13}O. The results of the delayed-proton measurements were compared with the known[48] decay of the mirror nucleus, ^{13}B, indicating a sizeable deviation from mirror symmetry in β-decay. The

short (9 ms) half-life of ^{13}O provided the main experimental difficulty. In order to reduce decay in transit, it was necessary to use less detector shielding than was used in the study of ^{17}Ne and ^{33}Ar.

A delayed-proton spectrum resulting from 43-MeV proton bombardment of nitrogen is shown in Fig. 16. All the peaks possessed half-lives of less than 50 ms, eliminating all known delayed-proton emitters except ^{13}O as the source of the activity. A second spectrum containing seven times fewer counts exhibited all the peaks shown except those at 3.44 and 6.38 MeV. Due to the poor statistics in the second experiment, the existence of these two peaks has been left an open question. For the purpose of subsequent analysis, they have been assumed to exist, but they are so weak that any error from this source would be small.

An energy scale was established by assuming that those peaks with unbracketed energies in Fig. 16 correspond to decays from known[79] states in ^{13}N. With this assumption, all the observed proton groups, with the exception of the two discussed above, were found to correspond to other known ^{13}N levels. In addition the widths of the proton groups, after correction for β-recoil broadening effects, were compatible with known[79] level widths. The proton peak energies and intensities are listed in Table XVI and the proposed decay scheme is shown in Fig. 17.

The proton branching ratios can be compared with proton resonance data in this case. The fraction of decays of the 8.92- and 9.52-MeV states that go to the ground state of ^{12}C is 0.70 ± 0.07 and 0.65 ± 0.12, respectively. This is in excellent agreement with the results from elastic and inelastic proton scattering[88] on ^{12}C where Γ_{el}/Γ was found to be 0.66 and

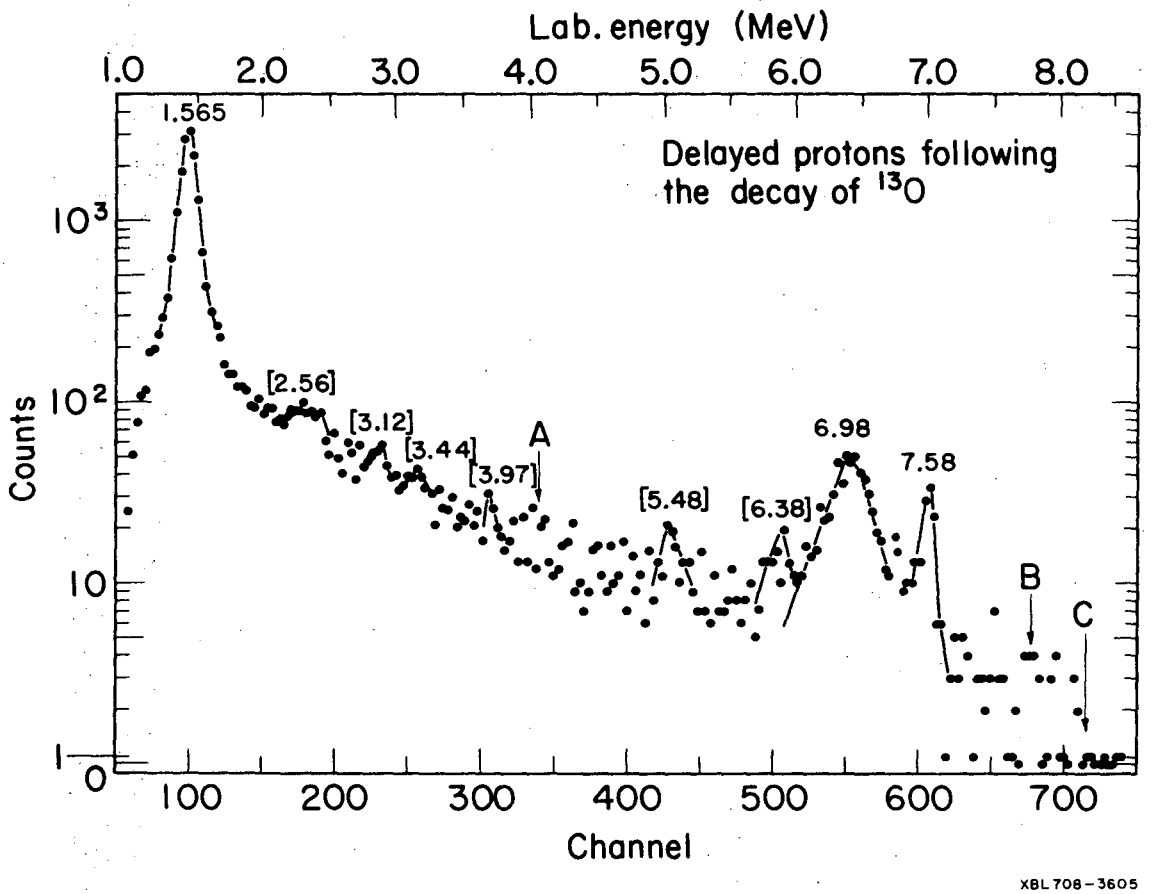

Fig. 16. Delayed proton spectrum following 43-MeV proton bombardment of nitrogen. The arrows indicate allowed but unobserved decays. The unbracketed energies were used to calibrate the spectrum.

Table XVI. Beta-decay of ^{13}O and a comparison with its mirror, ^{13}B.

^{13}N State (MeV)[a]	J^{π}	E_p(c.m.) (MeV)	Relative Intensity	% of all β-decays[b]	^{13}O log ft[b]	^{13}B log ft[c]
g.s.	$1/2^-$	-	-	88.1 ± 3.4	4.10 ± 0.02	4.04 ± 0.01
3.509	$3/2^-$	1.565[d]	100	10.7 ± 3.1	4.52 ± 0.13	4.45 ± 0.05
7.387	$5/2^-$	1.010[e] 5.48 ± 0.05	3.4 ± 1.4[f] 0.33 ± 0.10	0.40 ± 0.19	5.22 ± 0.23	5.33 ± 0.09
8.92	$1/2^-$	2.56 ± 0.05 6.98[d]	1.5 ± 0.3 3.5 ± 0.3[g]	0.54 ± 0.16	4.73 ± 0.14	4.59 ± 0.08
9.52	$3/2^-$	3.12 ± 0.05 7.58[d]	0.43 ± 0.15 0.8 ± 0.1[g]	0.13 ± 0.04	5.18 ± 0.14	> 5.0
10.35	$5/2^-$	3.97 ± 0.05 8.41[e]	0.13 ± 0.07 0.05 ± 0.03[f]	0.019 ± 0.012	5.8 ± 0.3	-
		3.44 ± 0.05[h]	0.3 ± 0.1	0.030 ± 0.016		
		6.38 ± 0.05[h]	0.46 ± 0.10	0.050 ± 0.018		

(continued)

Table XVI (continued)

[a]Energies, spins, and parities taken from Ref. 79.

[b]The ground state ft was taken to be 1.15 times that of ^{13}B and the mass excess of ^{13}O was taken to be 23.105 MeV (Refs. 46 and 49).

[c]Calculated from the data of Ref. 48 using a ^{13}B half-life of 17.33 ± 0.17 ms.

[d]Used to determine the energy calibration.

[e]Calculated value, unobserved in this experiment.

[f]Calculated using the known ratio of the elastic and inelastic widths.

[g]These relative intensities agree with those of Ref. 23 for the two peaks observed in that work.

[h]Weak proton groups observed in this work, but not positively attributed to ^{13}O decay.

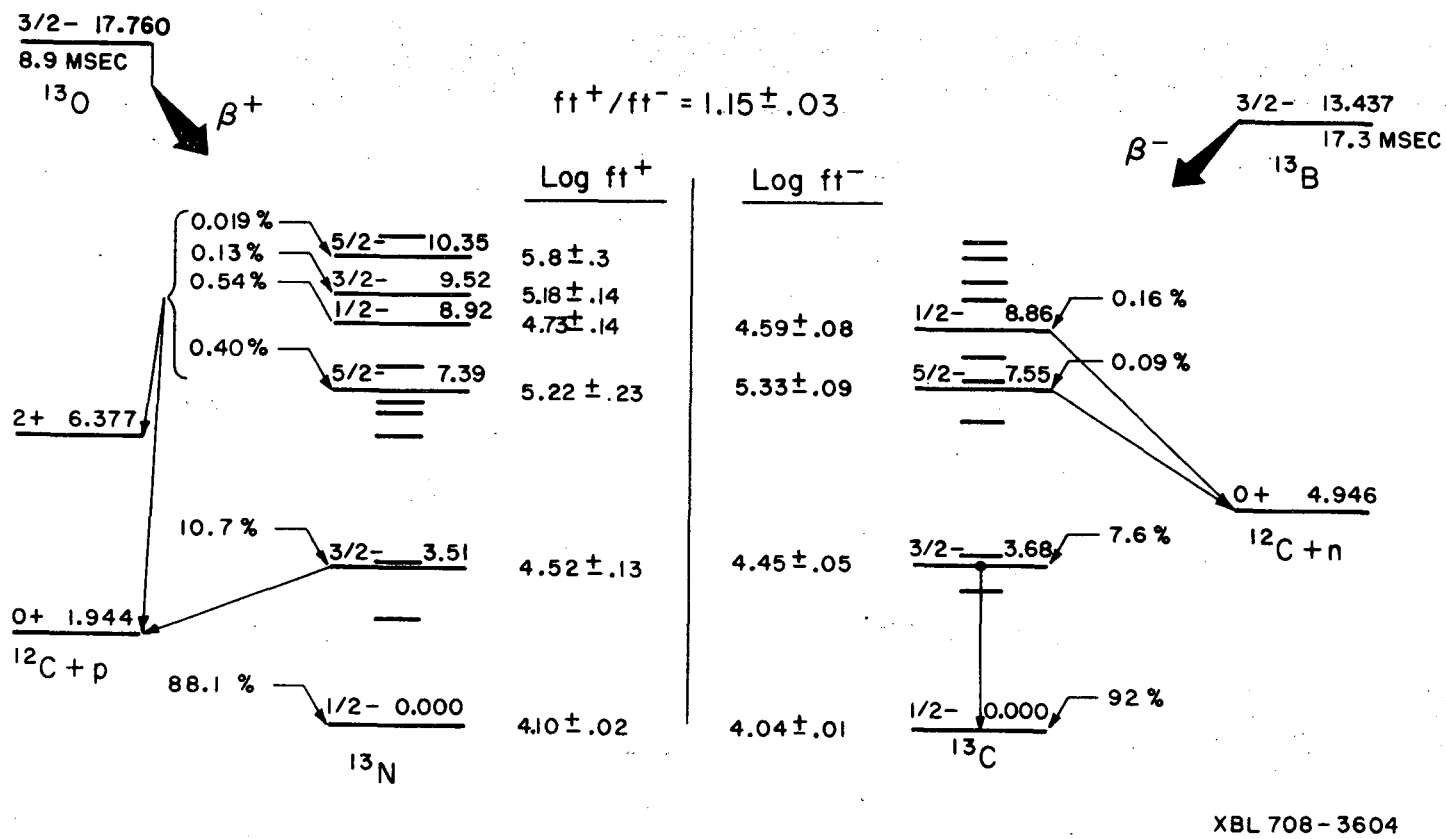

Fig. 17. Decay schemes of the mirror nuclei ^{13}B and ^{13}O. The half-life of ^{13}O and its β-decay properties result from this work, while the remainder of the figure represents the work of others.

0.58, respectively. This agreement justifies the use of Γ_{el}/Γ values from such experiments to renormalize the data in those cases where only one of two possible decay branches was observed. In particular, the protons following decay of the 7.39-MeV state in ^{13}N to the first excited state of ^{12}C are not energetic enough to penetrate the 14 μm ΔE detector. However, the known[88,89] Γ_{el}/Γ of 0.09 ± 0.02 suffices to determine the total number of protons de-exciting that state. Similarly the Γ_{el}/Γ[90,91] of 0.27 ± 0.02 for the 10.35-MeV level was used to renormalize the observed proton intensity. In this case only the decay to the first excited state was observed. Arrow B in Fig. 16 marks the predicted location of the ground-state branch. Its apparent absence is consistent with the known proton branching and the weakness of the β-decay branch. Arrows A and C mark the predicted locations of the unobserved protons from the $J^{\pi} = 1/2^{-}$, 10.78-MeV state.

This case is similar to that of ^{33}Ar in that the experimental observations include all significant β-transitions except that to the ground state. In this case however, as can be seen from Fig. 17, the available data from the decay of the mirror nucleus provide ft-values for all except two very weak decay branches. The relative intensities of Jones et al.[48] and a recent half-life measurement[50] were used to calculate ft-values for the decay of ^{13}B. These results, listed in Table XVI, were then used to predict an ^{13}O half-life of 7.74 ± 0.16 ms. This is not in agreement with the measured half-life of 8.9 ± 0.2 ms. (See Table II.)

This disagreement indicates a large violation of mirror symmetry in β-decay. Therefore, since Eq. (22) indicates that the possible cause

of mirror asymmetry is state independent, all the predicted ft-values should be increased by the ratio of the true to predicted half-lives, or by a factor of 1.15 ± 0.03. This was done for the ground state transition and then ft-values were calculated for the remaining decays. The results are listed in Table XVI. All the remaining transitions have log ft's that compare well with their mirrors, thus lending credence to the entire procedure.

Table XVI shows that allowed log ft's have been attributed to the β^+-transitions to all known[79] states in ^{13}N through 10.35 MeV which have $J^\pi = 5/2^-$, $3/2^-$, or $1/2^-$. This fixes the J^π of ^{13}O as $3/2^-$, in agreement with the simple shell model. Intermediate coupling calculations do not predict the $J^\pi = 5/2^-$, 10.35-MeV state.[92] Its existence has been ascribed to the excitation of two nucleons from the 1p-shell into the 1d-shell.[93] The high log ft-value for the β-transition to this state lends support to this supposition.

D. ^9C Decay

Figures 18 and 19 show the proton spectra obtained after 43-MeV proton bombardment of targets made by pressing ^{10}B-enriched boric acid into tungsten screens. Neither spectrum resembles any of the ones shown previously. Since all the other spectra had very low backgrounds, the continuum must be composed almost entirely of protons. ^{13}O could have been produced on a possible nitrogen contaminant in the oxygen sweeping gas, but its short half-life makes any contribution to the spectra from that source unlikely.

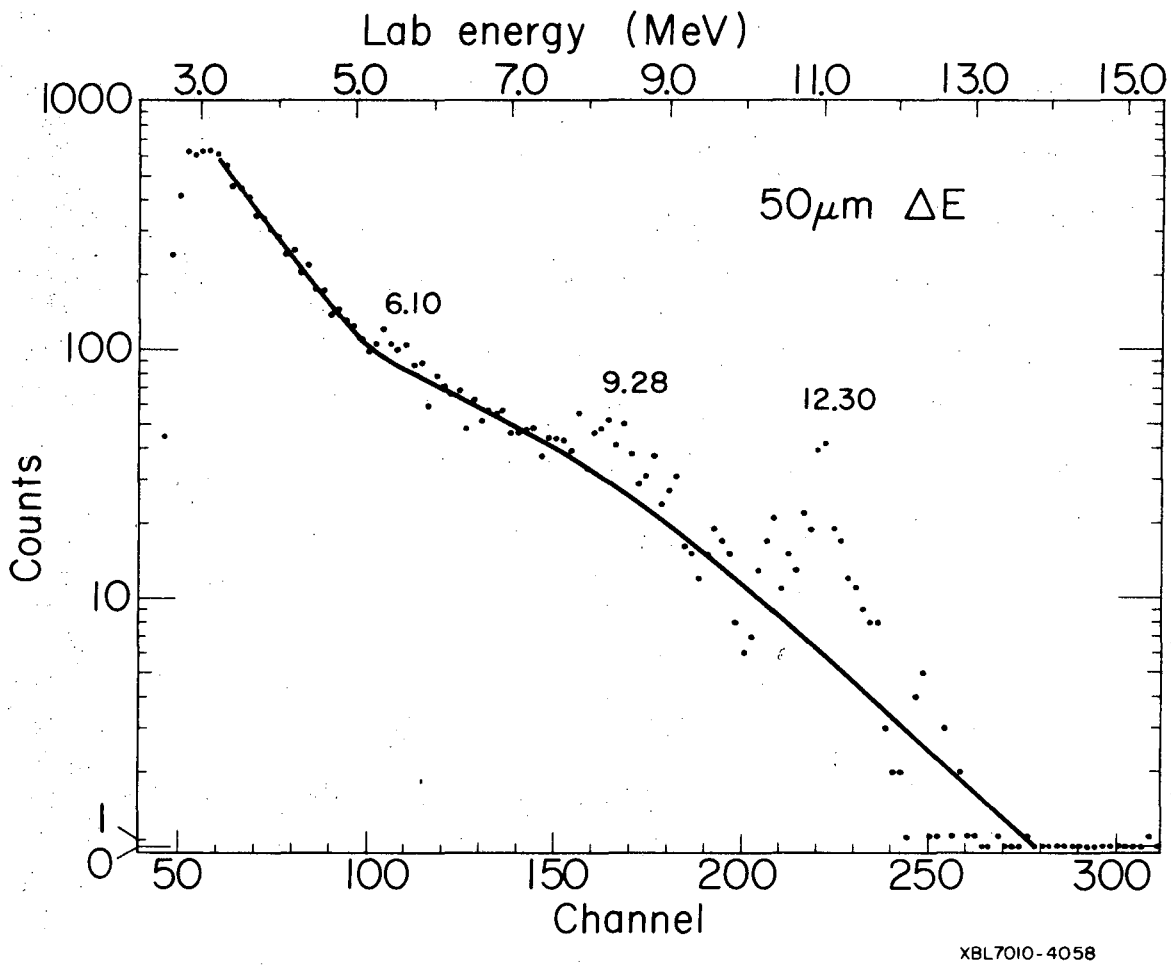

Fig. 18. Spectrum of identified delayed-protons observed following a 43-MeV proton bombardment of ^{10}B-enriched boric acid. The line is an empirical smooth curve fitting the continuum and is to guide the eye only.

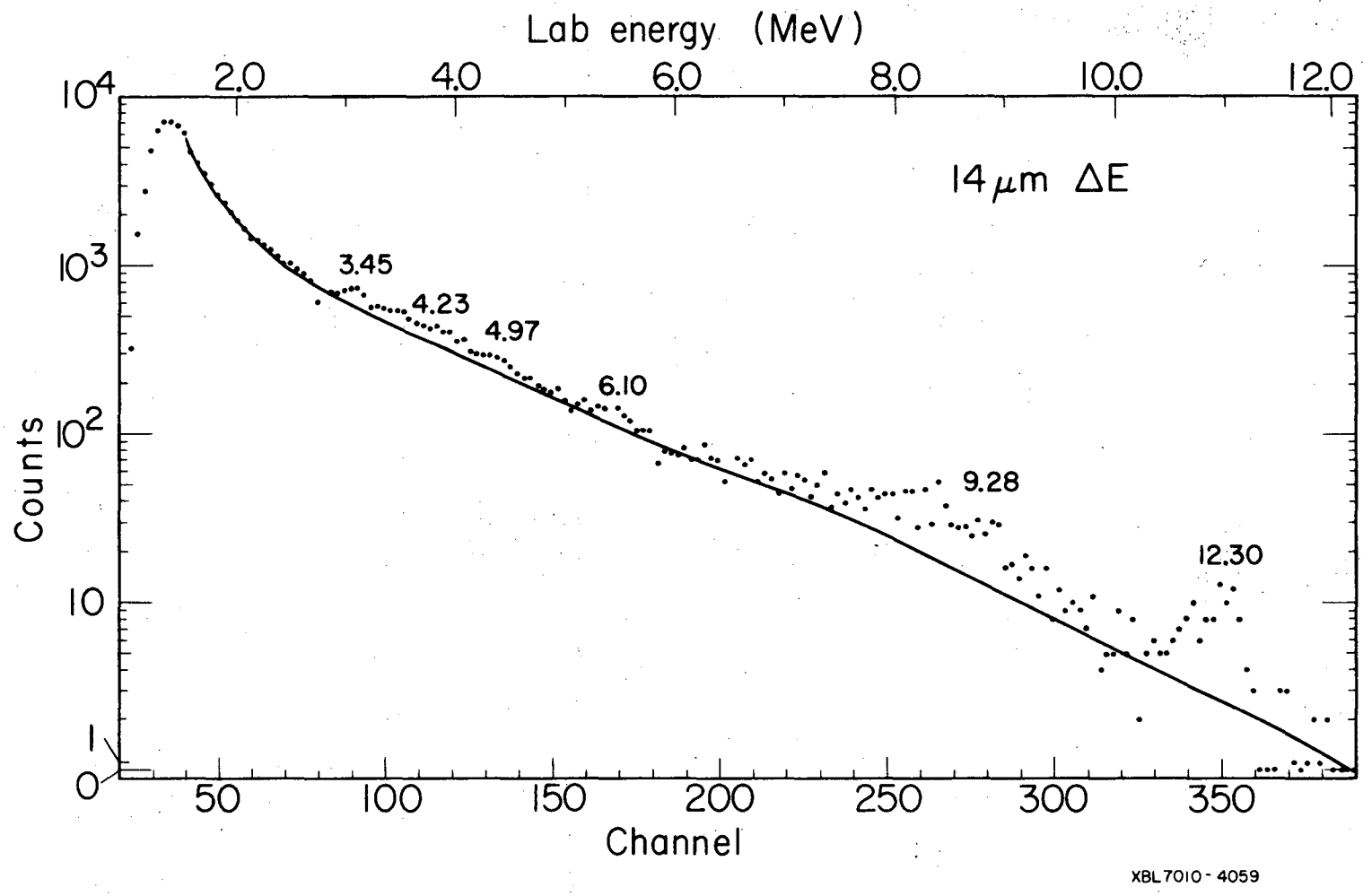

Fig. 19. Spectrum of identified delayed-protons taken under similar conditions to those of Fig. 18 except that a 14μm ΔE counter was used.

A ^{17}Ne spectrum taken just previously to the data in Fig. 18 calibrated the three peaks shown. Those peaks were then used to provide an internal energy scale for the data of Fig. 19. The line on both figures represents an attempt to draw a smooth curve that fits the continuum. The energies of all proton peaks are listed in Table XVII.

Table XVII also tentatively correlates the observed proton peaks with known[94] levels in ^{9}B. Figure 20 shows the known levels of ^{9}B and the many possible decay channels. The 4.97-MeV proton group has been assigned to a state that would be fed by a first-forbidden β-transition. This certainly seems unlikely. However the log ft-values for allowed decays in the mirror nucleus, ^{9}Li, range[45] from 5 to 6 while first-forbidden transitions in ^{11}Be and ^{15}C exhibit comparable log ft's, ranging from 6 to 6.8. Wilkinson et al.[95] populated levels in ^{9}B via the ^{10}B(He^{3},α)^{9}B reaction and observed α-p coincidences. They found that the 2.80-MeV state ($J^{\pi} = 3/2^{+}$, $5/2^{+}$) in ^{9}B decays almost entirely via proton emission to the ground state of ^{8}Be, while the 2.34-MeV state ($J^{\pi} = 5/2^{-}$, $1/2^{-}$) decays this way < 0.5% of the time. If this selectivity in decay channel were characteristic of all low lying states, it would be much easier to detect protons from the positive parity levels, even if they were fed via first-forbidden β-decay. Similarly, an unknown positive parity state may be the origin of the 6.10-MeV proton group.

It should be noted that virtually all the states shown in Fig. 20 have sizeable widths; in particular, both levels in ^{5}Li and the excited states of ^{8}Be are very broad. The strong continuum has two probable sources. The levels in ^{9}B are quite broad and so is the first excited

Table XVII. Delayed protons following the beta-decay of $^{9}C(J^{\pi} = 3/2^{-})$.

Proton Energy[a] (MeV)	Γ[b] (keV)[a]	Corresponding state in ^{9}B if decaying to: (MeV) ^{8}Be(g.s.)	^{8}Be(2.9 MeV)	Known state (MeV)	J^{π}
3.45 ± 0.25	200 ± 100	3.26 ± 0.25	c	(3.2)	$(3/2^{-})$
4.23 ± 0.25	1000 ± 200	4.04 ± 0.25	6.95 ± 0.25	4.05	$(5/2^{-})$
4.97 ± 0.15	400 ± 150	4.78 ± 0.15	c	4.85	$(3/2,5/2)^{+}$
6.10 ± 0.10	400 ± 100	5.91 ± 0.10	c		
9.28 ± 0.24[d]	1800 ± 200	9.09 ± 0.24	11.99 ± 0.24	12.06	$(1/2,3/2)^{-}$
12.30 ± 0.10[d]	450 ± 100	12.11 ± 0.10	c	12.06	$(1/2,3/2)^{-}$

[a]Energies and widths are given in the center-of-mass system.

[b]The width given is the full width at half maximum.

[c]The relatively narrow width indicates that the proton-group does not lead to the first excited state of $^{8}Be(\Gamma = 1.4$ MeV).

[d]The ratio of the intensities of the 9.28- and 12.30-MeV groups is 1.0 ± 0.2.

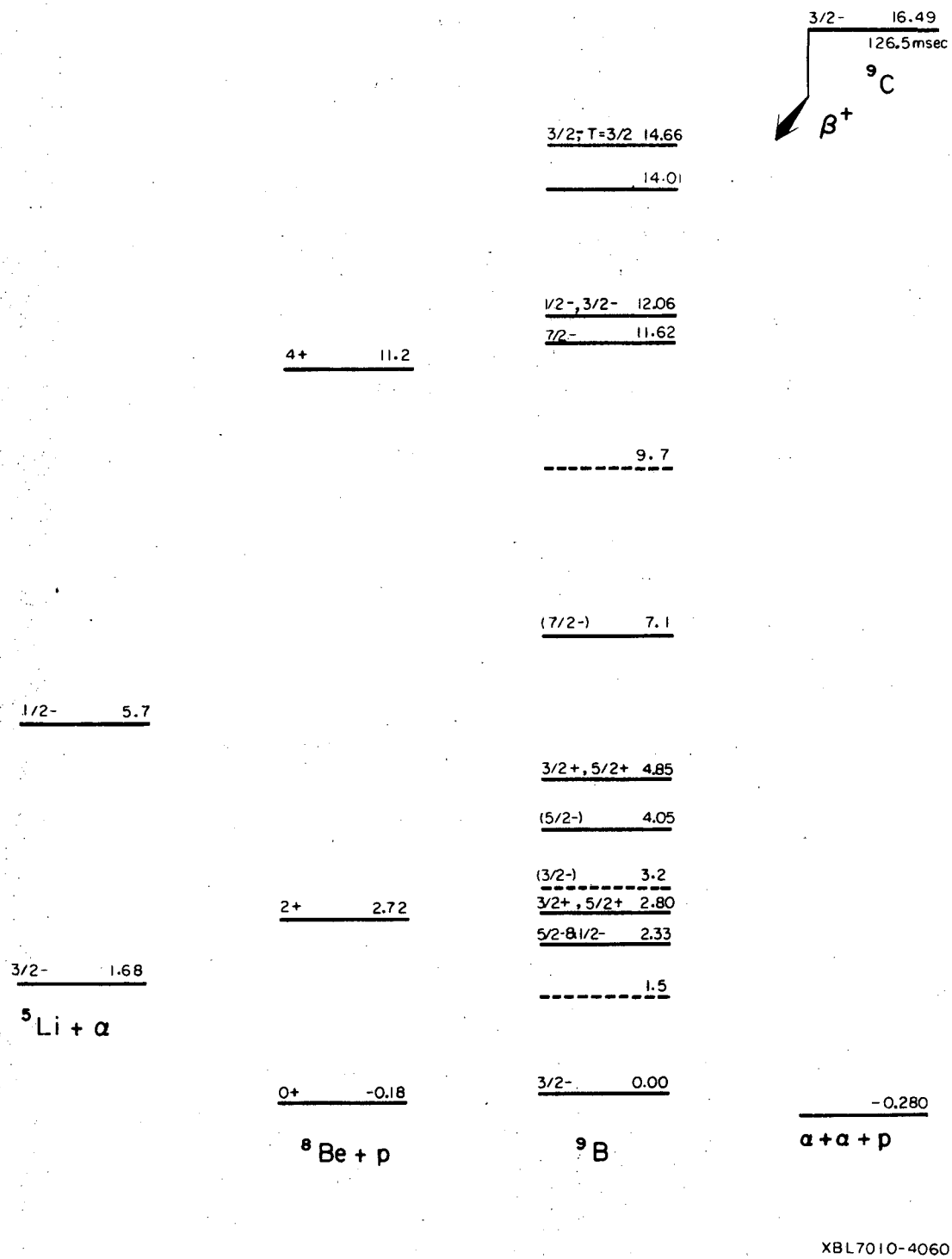

Fig. 20. A level diagram showing the complex decay channels available to states in ^{9}B. The level information comes from Refs. 6 and 93.

state of ^{8}Be (1.4 MeV). The resulting combination of broad peaks of varying amplitude could produce a featureless spectrum. Also, if a significant fraction of the levels in ^{9}B decay by α-emission, the proton spectrum following ^{5}Li breakup will be extremely wide. In any event singles delayed-proton measurements following ^{9}C decay are unable to determine ft-values and energy levels, in contrast to the other reported decays.

V. CONCLUSIONS

A. Isospin Purity

In Sec. II A, the relationship between superallowed ft-values and isospin purity was discussed. It was pointed out that a comparison between calculated and experimental values is a good method for determining isospin impurities. The results presented in Sec. IV contain experimental ft-values for superallowed transitions to T = 3/2 states in ^{17}F and ^{33}Cl. They are listed in Table XVIII along with experimental ft-values derived from the work of others for superallowed decays to ^{21}Na and ^{29}P.

The ft-values for the superallowed transitions to ^{21}Na and ^{29}P were obtained in similar ways. Both of these transitions are followed by proton emission, and have been observed in this way.[28] The only difficulty in determining the ft-values lies in calculating the strength of the decays to those states below the proton separation energy. Fortunately the mirror decays of $^{55}\,^{21}F$ and $^{56,58,59}\,^{29}Al$ are known. These mirror ft-values were corrected for the mirror asymmetry in β-decay by using the line in Fig. 1. They were then used to estimate the β-decay strength to proton-stable states in ^{21}Na and ^{29}P. The remainder of the strength for each nucleus was then assumed to go to proton-emitting states. The ft-values for the superallowed transitions could then be determined from the relative intensities in the delayed proton spectra.[28] The results are shown in Table XVIII.

The isospin purity of each analogue state listed in Table XVIII was then calculated using Eqs. (5) and (1). The calculations were done using two different assumptions: 1) the Gamow-Teller matrix elements were taken to be those of Ref. 36, and 2) the $\langle\sigma\rangle^2$ were taken to be zero. The

Table XVIII. Isospin purity of T = 3/2 states populated in superallowed β-decay.

Nucleus	ft-value to state (10^3 sec) Exp.	Calc.[a]	Limit[b]	Isospin purity(%)[c]
^{17}F	$1.93^{+0.17}_{-0.29}$	1.94	$\leqslant 2.05$	> 92
^{21}Na	3.3 ± 1.0[d]	1.83	$\leqslant 2.05$	50 ± 19[62 ± 19]
^{29}P	2.16 ± 0.21[e]	1.83	$\leqslant 2.05$	83 ± 9 [95^{+5}_{-9}]
^{33}Cl	2.18 ± 0.24	1.80	$\leqslant 2.05$	80 ± 10[94^{+6}_{-10}]

[a]The calculated values follow from use of Eq. (1) and the Gamow-Teller matrix elements of Ref. 36.

[b]The limit is arrived at by using Eq. (1) and assuming $\langle \sigma \rangle^2 = 0$.

[c]The bracketed value applies for $\langle \sigma \rangle^2 = 0$.

[d]This value was computed from the delayed-proton data of Ref. 28 using the ^{21}Mg half-life of Ref. 26. The strength of the β-transitions to those states in ^{21}Na below the proton separation energy was computed using the known[55] ft-values for the mirror decay and correcting for the energy dependence of the β-decay asymmetry as shown in Fig. 1.

[e]This value was computed using Refs. 28, 56, 58, and 59 in a similar way to that described in footnote d.

results are listed in Table XVIII. For all cases considered, except that of ^{17}F, there is an indication of significant isospin mixing if the Nilsson model values[36] of $\langle \sigma \rangle^2$ are used. Even for the other--unrealistic--assumption, $\langle \sigma \rangle^2 = 0$, there is a mild indication of isospin impurity in the analogue states of ^{29}P and ^{33}Cl, and considerable isospin mixing is still indicated for the lowest T = 3/2 state in ^{21}Na.

The calculation of the experimental ft-values in the cases of ^{21}Na, ^{29}P and ^{33}Cl contained the assumption that the line in Fig. 1 gives the proper amount of mirror asymmetry in β-decay. If larger violations of mirror symmetry were assumed, the calculated isospin purity would increase. Table II contains the values of δ, the asymmetry parameter, that result from assuming that isospin mixing does not occur. (If such a calculation were performed for mass 33, the resultant value of δ would be 10 ± 50, a meaningless number.) As a consequence of this assumption, the mirror asymmetries in the cases of mass 21 and mass 29 are the two largest listed in Table II and deviate considerably from the general trend of the data shown in Fig. 1. Thus, it is doubtful that mirror asymmetry in β-decay can be used to explain the entire discrepancy between the experimental and calculated values in Table XVIII.

Examination of the expanded section in Fig. 12 reveals another indication of isospin mixing in ^{33}Cl. There is a smooth progression from high ft-values for the states farthest away from the analogue state to lower ft-values for the nearby states. This phenomenon may be fortuitous, but it at least deserves further consideration. If β-decay to the four nearest states proceeds only via the T = 3/2 component (again using $\langle \sigma \rangle^2 = 0$), then the amplitude of that component can be calculated. The

resulting T = 3/2 strength is about 1% to 2% for each level, just about enough to explain the amount missing from the analogue state. Using Eq. (11), the charge-dependent matrix elements are found to range from 13 to 35 keV. This result is in agreement with the work of Bloom[96] in which the majority of charge-dependent matrix elements for 0^+ states were found to lie between 1 and 40 keV. Thus the proximity of these four levels to the analogue state may account for the observed isospin mixing. It must be noted, however, that two of the nearby states have unknown spin and parity, and mixing can only occur with $1/2^+$ states. Also the observed clustering of ft-values about the analogue state may be due to the presence of a T = 1/2 configuration at that energy which is simply related to the ^{33}Ar ground-state wave function.[97]

B. Antianalogue States

The state which has the same spatial configuration as a T = 3/2 analogue state, but which is coupled to T = 1/2, is called an antianalogue state. For example, the analogue state in ^{17}F is well described[87] by a $(1p_{1/2})$ hole coupled to the 0^+ ground state of ^{18}Ne to give a final J^π, T of $1/2^-$, 3/2. The antianalogue state consists of the same configuration coupled to T = 1/2. Since the antianalogue state has T = 1/2, it readily mixes with other T = 1/2 states of the same spin and parity. Thus, the antianalogue strength may be distributed among several levels.

For the case of ^{17}F, the antianalogue strength is expected[37] to be concentrated in the $1/2^-$ state at 3.105 MeV, a state fed surprisingly weakly in β-decay. This effect has been attributed to cancellations in

the β-decay matrix elements and a graph relating the ft-value for decay to this state to the percentage of antianalogue configuration therein has been obtained.[37] Using the graph and the ft-value from Table XV, the 3.105-MeV state contains between 80 and 85% of the antianalogue strength. The remainder is predicted to lie in a state at 6[87] or 8[37] MeV fed by a β-transition with a log ft-value of ∿ 3.5. The levels at 8.075, 8.437, and 8.825 are all possible candidates for this state, since they have log ft's of 3.96, 3.85, and 4.23 respectively.

While the data of Table XVIII do not indicate that the lowest ^{17}F, T = 3/2 state has any isospin impurity, it must have some impurities in its wave function to allow it to decay via proton emission. (Decay to ^{16}O + p is forbidden by isospin conservation, assuming the ^{16}O ground state is purely T = 0.) The antianalogue state is by definition very similar to the analogue state. The possible existence of some portion of its strength near the analogue state, as discussed above, suggests a possible source of the required mixing.

The wave function for the antianalogue state[37,87] consists of terms of the form $|(sd)^2(p_{1/2})^3\rangle$. Proton emission via antianalogue components mixed into the analogue state would then lead to states in ^{16}O with configurations $|(sd)^2(p_{1/2})^2\rangle$ or $|(sd)(p_{1/2})^3\rangle$. Theoretical calculations[98] indicate that the lowest 0^+, 1^-, 2^+, and 3^- states in ^{16}O have strong components of this type, while the first-excited 0^+ does not. Going farther, the total strength of these configurations for the first five states in ^{16}O is, in order, 34%, 0%, 66%, 29%, and 48%. The values of I/P in Table XIII reflect the reduced widths for the various proton decays

and are in reasonable agreement with the values predicted theoretically. Since the details of the wave functions have been neglected, any closer agreement cannot really be expected.

This indication of the strong role of the antianalogue configuration is corroborated by calculations[99] which predict the amount of T = 1/2 admixture in the T = 3/2 analogue state of ^{17}F. This calculation also predicted a < 1% total isospin impurity, in agreement with the present results.

Auerbach and Lev[100] considered only the effect of mixing with the antianalogue state in a calculation of proton widths of T = 3/2 analogue states in nuclei ranging from ^{13}N to ^{41}Sc. They achieved rough agreement with experiment, again illustrating the importance of the antianalogue state.

Even in the case of ^{33}Cl, for which the available wave functions[80] do not predict sufficient states, (see Sec. IV A), the antianalogue state may provide the observed mixing. About 23% of the antianalogue strength is predicted[80] to lie at ∿ 8 MeV. While this is not very close in energy to the 5.550-MeV, T = 3/2 state, this strength might move closer to the analogue state if the configurations that cause the additional levels were considered. In Sec. V A it was pointed out that the charge-dependent matrix elements calculated for those states near the ^{33}Cl analogue state agree well with those tabulated by Bloom.[96] Since many of the states Bloom considers are themselves antianalogue states, this agreement may be taken to indicate the presence of the antianalogue configuration in these nearby states.

VI. SUMMARY

A novel gas-sweeping system has been used to study various decay properties of ^{9}C, ^{13}O, ^{17}Ne, and ^{33}Ar. From these properties an indication of substantial isospin impurity in the T = 3/2 analogue state of ^{33}Cl was obtained. The antianalogue configuration may be responsible for this impurity. While no such large impurity was observed in ^{17}F, there are indications that the antianalogue configuration was responsible for the mixing which did occur.

Analysis of the decays of ^{9}C, ^{13}O, and ^{17}Ne provided evidence for mirror asymmetry in β-decay that corroborated several other observations of asymmetry. As discussed in Sec. II C, explanations of this effect postulate an induced tensor component in nuclear beta decay or the existence of meson exchange effects, or both.

Clearly further theoretical and experimental study of mirror asymmetry is warranted. In particular, additional study of the decay of ^{21}Mg is especially needed. At present the data indicate either a very large mirror asymmetry or a large isospin impurity in the analogue state. An improved delayed-proton spectrum and a concomitant improved half-life would reduce the error bars on the two derived quantities. Further, γ-ray measurements could yield information concerning the state-dependence of the mirror asymmetry and possibly absolute ft-values.

Both counting systems discussed in Sec. III have potential applications to different problems than those considered here. For example, the slotted-wheel system could be used to search for delayed-proton emission in the T = 3/2, A = 4n+3 series. The lightest known[101] member of

this unexplored series is ^{23}Al. An example of a possible use of the gas-sweeping system would be a detailed study of ^{34}Ar, which should decay primarily via a pure Fermi transition ($0^+ \rightarrow 0^+$). Undoubtedly many other such possibilities exist.

ACKNOWLEDGMENTS

The congenial and productive atmosphere at the 88-in. cyclotron has contributed greatly to the successful conclusion of this work. For this, I thank all those associated with the cyclotron during my stay there and particularly Dr. Bernard Harvey, the Director.

The able direction, advice, criticism, etc. of Dr. Joseph Cerny, my research director, is deeply appreciated.

For his encouragement, tolerance, and instruction during my first year of graduate study, I thank Dr. Sam Cosper.

I would like to give special thanks to Dr. John Hardy and Richard Sextro whose active collaboration has been essential to much of this work.

Thanks are also due to all those who helped in the data taking, particularly to John Macdonald whose extra interest and enthusiasm is appreciated.

I would like to thank Creve Maples for some interesting discussions and his help with various computer problems.

David Allred and Gary J. Ehrhardt, although associated with this work for only a short time, made significant contributions to it; for which I thank them.

Don Landis has been a constant help throughout the course of the work, creating various electronic devices upon short notice and explaining their operation with patience and clarity.

Most of all, I wish to thank my wife, Ronalie, and my three children. Seeing happy smiles upon returning home somehow makes it all worthwhile.

This work was done under the auspices of the United States Atomic Energy Commission.

APPENDIX A

Cross Section Formula

It is possible to extract absolute cross sections from the data obtained with the system in which a slotted rotating wheel protects the detectors during beam bursts. To do this it is necessary to correct for the fact that some of the activity recoils out of the target and is lost. Also corrections must be made that take account of decay during periods in which the target is not observed.

For each cycle of the rotating wheel, the number of nuclei produced, P, is given by

$$P = N \sigma \phi \quad , \tag{A-1}$$

where N is the number of target nuclei per cm^2, σ is the cross section, and ϕ is the number of beam particles per cycle. Taking account of the fact that some of the activity will recoil out of the target and be lost, N is given by

$$N = (t/\cos\theta - R) \frac{N^o (10)^{-3} F}{M} \quad , \tag{A-2}$$

where t is the target thickness in mg/cm^2, θ is the angle of target rotation, R is the recoil range of the activity, N^o is the Avogadro's number, M is the molecular weight of the target material, and F takes account of the number of target nuclei per molecule and of the isotope ratio. The recoil energy was calculated by assuming that the compound nucleus emitted the neutrons with zero energy in the center of mass system. Then recoil

ranges were interpolated from published tables.[67] For the gas targets, the effective target thickness was taken to be the recoil range plus a small correction for the amount of gas the counters could see behind the exit window.

The flux of beam particles per cycle is given by

$$\phi = \frac{Q}{Z_p \, e \, N_c} \quad , \tag{A-3}$$

where Q is the integrated charge for the entire run, Z_p is the atomic number of the projectile, e is the electron charge and N_c is the total number of wheel revolutions.

The wheel cycle consists of a bombarding time t_1, a delay and inspect time t_2, a counting time t_3, and another short delay to avoid counting when the beam reappears, t_4. At equilibrium the number of nuclei produced per cycle equals the number that decay. If N' is the equilibrium number of nuclei at the end of the bombardment time t_1, the equilibrium condition yields

$$P = N'(1 - e^{-\lambda T}) + [P - P/\lambda t_1 \, (1 - e^{-\lambda t_1})] \quad , \tag{A-4}$$

where T is the total wheel revolution time and λ is the appropriate decay constant. The term in the brackets represents the decay of those nuclei formed during the cycle, under the assumption that the beam intensity does not vary during the bombarding time.

The number, I, of nuclei observed during a counting period, t_2, is given, after solving Eq. (A-4) for N', as

$$I = \frac{G\ f\ P}{\lambda t_1}(1 - e^{-\lambda t_1})(e^{-\lambda t_2} - e^{-\lambda(t_2+t_3)})/(1 - e^{-\lambda T}) \quad , \quad \text{(A-5)}$$

where G is the geometry factor and f is the fraction of β-decays that go to a particular peak or peaks. Values of f were taken from the literature[29,31] for ^{25}Si and ^{41}Ti, from the present work for ^{17}Ne and from a calculation[36] for the ft-value of the superallowed transition in ^{21}Mg.

Since the number of counts given by Eq. (A-5) is seen for each cycle, the final expression for the cross section obtained by combining Eqs. (A-1, A-2, A-3, A-5) is

$$\sigma = C\ \lambda\ t_1(1 - e^{-\lambda T})\ M\ Z_p e/Q(t/\cos\theta - R)\ N^o(10)^{-3} F\ f$$

$$G(1 - e^{-\lambda t_1})(e^{-\lambda t_2} - e^{-\lambda(t_2+t_3)}) \quad , \quad \text{(A-6)}$$

where C is the number of observed events.

APPENDIX B

Beta-Broadening of the Delayed-Proton Peaks

In examining the influence of the initial β^+ on the energy of the delayed proton, the motion of the nucleus and the proton may be treated classically, while the electron must be treated relativistically. The application of conservation of momentum at the instant before proton emission, but after β^+-decay, gives the velocity of the recoiling nucleus as

$$V_R = W(1 + 2mc^2/W)^{1/2}/Ac \quad , \tag{B-1}$$

where W is the average β-particle energy for the transition of interest, m is the rest mass of the electron, and A is the mass of the recoiling nucleus. Equation (B-1) represents an estimate of the recoil velocity because the neutrino has been neglected, eliminating the complication introduced by the β-ν correlation. In the system consisting of the recoiling nucleus, the velocity of the emitted proton is

$$V_p = \frac{1}{m_p} \sqrt{2m_p(\frac{A-1}{A})E} \quad , \tag{B-2}$$

where m_p is the rest mass of a proton and E is its center-of-mass energy. Adding the two velocity vectors, with θ as the angle between them, the energy of the proton in the laboratory system is

$$E_L = m_p V_p^2/2 + m_p V_R^2/2 - m_p V_R V_p \cos\theta \quad . \tag{B-3}$$

The first term in Eq. (B-3) is the uncorrected proton energy, the second term would increase the observed energy but is negligibly small, and the

third term is the only one that will contribute additional width to the observed peak. Assuming an infinitely narrow natural line width, the full width at half maximum is given by

$$\mathrm{FWHM} = m_p V_p V_R \quad , \tag{B-4}$$

or

$$\mathrm{FWHM} = \frac{W}{Ac} \sqrt{\left(1 + \frac{2mc^2}{W}\right)} \sqrt{2m_p\left(\frac{A-1}{A}\right)E} \quad . \tag{B-5}$$

As can be seen from Eq. (B-5), the line width spreading is greatest for light mass nuclei and high energy decays--just those nuclei studied.

REFERENCES AND FOOTNOTES

1. R. J. Blin-Stoyle and M. Rosina, Nucl. Phys. 70, 321 (1965).
2. R. J. Blin-Stoyle in Isospin in Nuclear Physics, ed. by D. H. Wilkinson, (North-Holland, Amsterdam, 1969) p. 115.
3. D. H. Wilkinson, Phys. Letters 31B, 447 (1970).
4. J. N. Huffaker and E. Greuling, Phys. Rev. 132, 738 (1963).
5. J. Cerny, Ann. Rev. Nucl. Sci. 18, 27 (1968).
6. T. Lauritsen and F. Ajzenberg-Selove, Nucl. Phys. 78, 1 (1966).
7. H. Daniel, W. Collin, M. Kuntze, S. Margulies, B. Martin, O. Mehling, P. Schmidlin, and H. Schmitt, Nucl. Phys. A118, 689 (1968).
8. F. Ajzenberg-Selove and T. Lauritsen, Nucl. Phys. A114, 1 (1968).
9. D. Schwalm and B. Povh, Nucl. Phys. 89, 401 (1966).
10. F. Ajzenberg-Selove, Nucl. Phys. (to be published).
11. H. Hättig, K. Hünchen, P. Roth, and H. Wäffler, Nucl. Phys. A137, 144 (1969).
12. G. J. Clark, P. B. Treacy, and S. N. Tucker, Australian J. Phys. 22, 663 (1969).
13. R. M. Policher, J. E. Steigerwalt, J. W. Sunier, and J. R. Richardson, Phys. Rev. 163, 1084 (1967).
14. J. W. Sunier, A. J. Armini, R. M. Policher, and J. R. Richardson, Phys. Rev. 163, 1091 (1967).
15. N. S. Oakey and R. D. Macfarlane, Phys. Rev. Letters 25, 170 (1970).
16. A. J. Armini, J. W. Sunier, and J. R. Richardson, Phys. Rev. 165, 1194 (1968).
17. J. E. Steigerwalt, J. W. Sunier, and J. R. Richardson, Nucl. Phys. A137, 585 (1969).

18. A. J. Armini, J. W. Sunier, R. M. Policher, and J. R. Richardson, Phys. Letters 21, 335 (1966).

19. D. F. Torgerson, N. S. Oakey, and R. D. Macfarlane, Bull. Am. Phys. Soc. 15, 30 (1970).

20. R. I. Verrall and R. E. Bell, Nucl. Phys. A127, 635 (1969).

21. J. C. Hardy, R. I. Verrall, R. Barton, and R. E. Bell, Phys. Rev. Letters 14, 376 (1965).

22. J. M. Mosher, R. W. Kavanagh, and T. A. Tombrello, Phys. Rev. C 3, 438 (1971).

23. R. McPherson, R. A. Esterlund, A. M. Poskanzer, and P. L. Reeder, Phys. Rev. 140, B1513 (1965).

24. R. McPherson, J. C. Hardy, and R. E. Bell, Phys. Letters 11, 65 (1964).

25. R. W. Fink, T. H. Braid, and A. M. Friedman, Arkiv Fysik 36, 471 (1967).

26. J. C. Hardy and R. E. Bell, Can. J. Phys. 43, 1671 (1965).

27. R. A. Esterlund, R. McPherson, A. M. Poskanzer, and P. L. Reeder, Phys. Rev. 156, 1094 (1967).

28. R. I. Verrall, Ph.D. thesis, McGill University (1968), (unpublished).

29. P. L. Reeder, A. M. Poskanzer, R. A. Esterlund, and R. McPherson, Phys. Rev. 147, 781 (1966).

30. J. C. Hardy and R. I. Verrall, Phys. Letters 13, 148 (1964).

31. A. M. Poskanzer, R. McPherson, R. A. Esterlund, and P. L. Reeder, Phys. Rev. 152, 995 (1966).

32. J. C. Hardy and R. I. Verrall, Can. J. Phys. 43, 418 (1965).

33. J. C. Hardy and R. I. Verrall, Phys. Rev. Letters 13, 764 (1964).

34. J. Cerny, C. U. Cardinal, H. C. Evans, K. P. Jackson, and N. A. Jelley, Phys. Rev. Letters 24, 1128 (1970).

35. R. J. Blin-Stoyle and J. M. Freeman, Nucl. Phys. A150, 369 (1970), and references therein.

36. J. C. Hardy and B. Margolis, Phys. Letters 15, 276 (1965).

37. B. Margolis and N. de Takacsy, Phys. Letters 15, 329 (1965).

38. M. G. Silbert and J. C. Hopkins, Phys. Rev. 134, B16 (1964).

39. H. F. Schopper, Weak Interactions and Nuclear Beta-Decay, (North-Holland, Amsterdam, 1966).

40. J. P. Davidson, Jr., Phys. Rev. 82, 48 (1951).

41. R. P. Feynman and M. Gell-Mann, Phys. Rev. 109, 193 (1958).

42. S. Weinberg, Phys. Rev. 112, 1375 (1958).

43. R. J. Blin-Stoyle and S. C. K. Nair, Advan. Phys. 15, 493 (1966).

44. M. Goldberger and S. Treiman, Phys. Rev. 111, 354 (1958).

45. Y. S. Chen, T. A. Tombrello, and R. M. Kavanagh, Nucl. Phys. A146, 136 (1970).

46. G. F. Trentelman, B. M. Preedom, and E. Kashy, Phys. Rev. Letters 25, 530 (1970).

47. I. Dostrovsky, R. Davis, Jr., A. M. Poskanzer, and P. L. Reeder, Phys. Rev. 139, B1513 (1965).

48. K. W. Jones, W. R. Harris, M. T. McEllistrem, and D. E. Alburger, Phys. Rev. 186, 978 (1969).

49. R. Mendelson, G. J. Wozniak, A. D. Bacher, J. M. Loiseaux, and J. Cerny, Phys. Rev. Letters 25, 533 (1970).

50. D. E. Alburger and D. H. Wilkinson, private communication.

51. D. E. Alburger and D. H. Wilkinson, Phys. Letters 32B, 190 (1970).

52. E. Aslanides, F. Jundt, and A. Gallman, Nucl. Phys. A152, 251 (1970).

53. D. H. Wilkinson and D. E. Alburger, Phys. Rev. Letters 24, 1134 (1970).

54. J. L. C. Ford, Jr., J. K. Bair, C. M. Jones, and H. B. Willard, Nucl. Phys. 63, 588 (1965); P. Kienle and K. W. Wien, Nucl. Phys. 41, 608 (1963); and M. E. Bunker, M. G. Silbert, J. W. Starner, R. K. Sheline, and N. Jarmie, Bull. Am. Phys. Soc. 8, 317 (1963).

55. W. R. Harris and D. E. Alburger, Phys. Rev. C 1, 180 (1970).

56. A. D. W. Jones, J. A. Becker, R. E. McDonald, and A. R. Poletti, Phys. Rev. C 1, 1000 (1970).

57. D. E. Alburger and G. A. P. Engelbertink, Phys. Rev. C 2, 1594 (1970), and references therein; A. Wyttenbach and H. Dulakas, J. Radioanal. Chem. 2, 287 (1969).

58. P. M. Endt and C. Van der Leun, Nucl. Phys. A105, 1 (1967).

59. W. R. Harris, K. Nagatani, and D. E. Alburger, Phys. Rev. 187, 1445 (1969).

60. G. I. Harris and A. K. Hyder, Jr., Phys. Rev. 157, 958 (1967).

61. H. J. Strubbe and D. K. Callebaut, Nucl. Phys. A143, 537 (1970).

62. D. H. Wilkinson and B. E. F. Macefield, Nucl. Phys. A158, 110 (1970).

63. D. H. Wilkinson, Nucl. Phys. A158, 476 (1970).

64. J. Delorme and M. Rho, Phys. Letters 34B, 238 (1971).

65. H. J. Lipkin, Phys. Letters 34B, 202 (1971).

66. G. W. Butler, J. Cerny, S. W. Cosper, and R. L. McGrath, Phys. Rev. 166, 1096 (1968).

67. L. C. Northcliffe and R. F. Schilling, Nucl. Data A7, 233 (1970).

68. F. S. Goulding, D. A. Landis, J. Cerny, and R. H. Pehl, Nucl. Instr. Methods 31, 1 (1964).

69. H. L. Scott and D. M. Van Patter, Phys. Rev. 184, 1111 (1969).

70. I would like to thank John Hardy for doing these calculations.

71. C. M. Lederer, J. M. Hollander, and I. Perlman, Table of Isotopes, (John Wiley and Sons, Inc., New York, 1967).

72. J. B. Cumming, in Applications of Computers to Nuclear and Radiochemistry, ed. by G. D. O'Kelley (Office of Technical Services, Washington, D. C. 1963), NAS-NS 3107.

73. P. L. Reeder, A. M. Poskanzer, and R. A. Esterlund, Phys. Rev. Letters 13, 767 (1964).

74. R. Van Bree, H. Ogata, and G. M. Temmer, Bull. Am. Phys. Soc. 13, 1402 (1968).

75. D. H. Youngblood, G. C. Morrison, and R. E. Segel, Phys. Letters 22, 625 (1966); B. Teitelman and G. M. Temmer, Phys. Letters 26B, 371 (1968).

76. C. E. Moss, Nucl. Phys. A145, 423 (1970).

77. J. W. Gordon, Thesis, University of Kansas (unpublished).

78. W. T. Sharp, H. E. Gove, and E. B. Paul, Atomic Energy of Canada Ltd., AECL-268 (unpublished).

79. F. Ajzenberg-Selove, Nucl. Phys. A152, 1 (1970).

80. P. W. M. Glaudemans, G. Wiechers, and P. J. Brussard, Nucl. Phys. 56, 548 (1964).

81. S. R. Salisbury and H. T. Richards, Phys. Rev. 126, 2147 (1962). A correction for errors in the calibration of the analysis magnet used by the above authors has been applied to the energies they originally reported. (J. C. Davis, private communication.)

82. R. W. Harris, G. C. Phillips, and C. M. Jones, Nucl. Phys. 38, 259 (1962).

83. R. L. Dangle, L. D. Opplinger, and G. Hardie, Phys. Rev. 133B, 647 (1964). The correction mentioned for Ref. 81 applies here as well.

84. V. Gomes, R. A. Douglas, T. Polga, and O. Sala, Nucl. Phys. 68, 417 (1965).

85. J. R. Patterson, H. Winkler, and C. S. Zaidins, Phys. Rev. 163, 1051 (1967).

86. C. P. Browne and I. Michael, Phys. Rev. 134B, 133 (1964).

87. B. Margolis and N. deTakacsy, Can. J. Phys. 44, 1431 (1966).

88. A. C. L. Barnard, J. B. Swint, and T. B. Clegg, Nucl. Phys. 86, 130 (1966).

89. G. G. Shute, D. Robson, V. R. McKenna, and A. T. Berztiss, Nucl. Phys. 37, 535 (1962); F. C. Barker, G. D. Symons, N. W. Tanner, and P. B. Treacy, Nucl. Phys. 45, 449 (1963); and N. Nikolic, L. J. Lidofsky, and T. H. Kruse, Phys. Rev. 132, 2212 (1963).

90. E. M. Bernstein and G. E. Terrell, Phys. Rev. 173, 937 (1968).

91. J. B. Swint, J. S. Duval, Jr., A. C. L. Barnard, and T. B. Clegg, Nucl. Phys. A93, 177 (1967).

92. S. Cohen and D. Kurath, Nucl. Phys. 73, 1 (1965).

93. D. Kurath, private communication referred to in Ref. 91.

94. K. Gul, B. H. Armitage, and B. W. Hooton, Nucl. Phys. A153, 390 (1970); A. S. Clough, C. J. Batty, B. E. Bonner, and L. E. Williams, Nucl. Phys. A143, 385 (1970); and references therein.

95. D. H. Wilkinson, J. T. Sample, and D. E. Alburger, Phys. Rev. 146, 662 (1966).

96. S. D. Bloom in Isobaric Spin in Nuclear Physics, ed. by J. D. Fox and D. Robson, (Academic Press Inc., New York, 1966) p. 123.

97. V. A. Karnaukhov, Yad. Fiz. 10, 450 (1969); translation Sov. J. Nucl. Phys. 10, 257 (1970).

98. A. P. Zuker, B. Buck, and J. B. McGrory, Phys. Rev. Letters 21, 39 (1968).

99. G. E. Walker and D. Schlobohm, Nucl. Phys. A140, 49 (1970).

100. N. Auerbach and A. Lev, Phys. Letters 34B, 13 (1971).

101. J. Cerny, R. A. Mendelson, Jr., G. J. Wozniak, J. E. Esterl, and J. C. Hardy, Phys. Rev. Letters 22, 612 (1969).

LEGAL NOTICE

This report was prepared as an account of work sponsored by the United States Government. Neither the United States nor the United States Atomic Energy Commission, nor any of their employees, nor any of their contractors, subcontractors, or their employees, makes any warranty, express or implied, or assumes any legal liability or responsibility for the accuracy, completeness or usefulness of any information, apparatus, product or process disclosed, or represents that its use would not infringe privately owned rights.

TECHNICAL INFORMATION DIVISION
LAWRENCE RADIATION LABORATORY
UNIVERSITY OF CALIFORNIA
BERKELEY, CALIFORNIA 94720